Solar Energy Supply and Storage for the Legacy and Nonlegacy Worlds

Timothy R. Cook, Dilek K. Dogutan, Steven Y. Reece, Yogesh Surendranath, Thomas S. Teets, and Daniel G. Nocera*

Department of Chemistry, 6-335, Massachusetts Institute of Technology, 77 Massachusetts Avenue, Cambridge, Massachusetts 02139-4307, United States

Received August 2, 2010

Contents

1. Setting the Scope of the Challenge

1.1. The Need for Solar Energy Supply and Storage

The energy appetite of our global society is enormous. Worldwide primary energy consumption in 2007 was 483.59668 Quad BTU (458×10^{18} joules), which is an average energy consumption rate of 16.2 terrawatts (TW, one TW equals 10^{12} watts, or 10^{12} joules per second).[1] Global energy need will roughly double by midcentury and triple

Timothy R. Cook was born on September 16, 1982, and grew up in Moretown, Vermont. In 2001, he began studies at Boston University, earning a B.A. in Chemistry while working in the laboratory of Prof. John P. Caradonna. In the fall of 2005, he began graduate school in the laboratory of Prof. Daniel G. Nocera at the Massachusetts Institute of Technology, focusing on molecular approaches for solar energy conversion, specifically photochemical halogen production. Tim began a postdoctoral appointment at the University of Utah in the laboratory of Prof. Peter J. Stang in the summer of 2010.

Dilek K. Dogutan, was born and grew up in Erenköy/Istanbul, Turkey. She majored in Organic Chemistry at Middle East Technical University (METU). After graduating from METU, Dilek worked at pharmaceutical companies both in Istanbul, Turkey, and Munich, Germany, as a research scientist. She subsequently attended North Carolina State University and received her Ph.D. in Organic Chemistry under the mentorship of Professor Jonathan S. Lindsey. During her doctoral studies, Dilek worked on the development of new synthetic methodologies for variously substituted metalloporphyrins. Upon completion of her Ph.D. in 2008, she began a postdoctoral position at Massachusetts Institute of Technology under the direction of Professor Daniel G. Nocera.

* To whom correspondence should be addressed. E-mail: nocera@mit.edu.

10.1021/cr100246c
Published on Web 11/10/2010

Steve Y. Reece was born on February 26, 1980, and grew up in Kinston, North Carolina. He received his initial laboratory training with Prof. Durwin Striplin at Davidson College in Davidson, North Carolina (B.Sci., High Honors in Chemistry, 2002). Following this, he migrated north to Cambridge, Massachusetts, where he was mentored by Profs. Daniel Nocera and JoAnne Stubbe at the Massachusetts Institute of Technology (Ph.D., Davison Prize for best thesis, 2007). Longing for a west coast experience, he moved to Berkeley, California, where he studied nitric oxide and heme biochemistry under the guidance of Prof. Michael Marletta (UC Berkeley, postdoc, 2007−2009). In 2009, Steve returned to Cambridge, Massachusetts to help Prof. Nocera found Sun Catalytix and has since been working to commercialize novel, low-cost, renewable energy conversion and storage devices.

Yogesh (Yogi) Surendranath was born in Bangalore, India, on October 12, 1983. He grew up in Kent, a college town in northeastern Ohio, after immigrating to the United States at age 3. In 2006, he received a Bachelor of Science degree in Chemistry from the University of Virginia, where he conducted research in the laboratory of W. Dean Harman. He is currently a graduate student at MIT in the laboratory of Daniel G. Nocera, where he is supported by a fellowship from the National Science Foundation. Yogi's graduate research has focused on the study of electrocatalytic oxygen evolution mediated by metal oxide based thin film catalysts.

Tom Teets was born on June 13, 1984, and grew up in Amherst, OH, a small town near Cleveland. In 2007, he received a Bachelor of Science degree in Chemistry from Case Western Reserve University, where he received his first introduction to inorganic chemistry in the laboratory of Thomas G. Gray. He is currently a graduate student at MIT in Daniel G. Nocera's lab, where he is supported by a fellowship from the Fannie and John Hertz Foundation. Tom's graduate research has focused on the design of molecular constructs for photocatalytic hydrogen production and other small molecule transformations of relevance to renewable energy.

Daniel G. Nocera is the Henry Dreyfus Professor of Energy and Professor of Chemistry, Director of the Solar Revolutions Project, and Director of the Eni Solar Frontiers Center at MIT. He studies mechanisms of energy conversion in biology and chemistry with primary focus in recent years on the generation of solar fuels. He has discovered a solar fuels process that captures many of the elements of photosynthesis outside of the leaf. His recent efforts are devoted to bringing personalized, carbon-neutral energy to the poor and those of the nonlegacy world.

by 2100.[2−4] Much of this demand is driven by a growing world population, which is projected to increase from 6.2 billion in 2001 to approximately 9.4 billion by 2050.[5] In addition to these 3 billion new inhabitants of the planet, 3 billion people in the nonlegacy world seek a rising standard of living. Geopolitical, environmental, and economic security will likely only be realized by meeting the energy demand of these 6 billion additional energy users by supplying a sustainable and carbon-neutral energy source, and within the next 10−20 years. To do so will require invention, development, and deployment of carbon-neutral energy on a scale commensurate with, or larger than, the entire present-day energy supply from all sources combined.

To frame the problem illustratively, consider the analysis summarized in Table 1,[6] which lists the per capita energy consumption of selected regions as of 2007 multiplied by the projected global population of 9.4 billion people for the year 2050. This product is the amount of energy that will be needed in 2050, on average, based on that country's energy consumption in 2007. For example, if 9.4 billion people adopted the current standard of living for a U.S. resident (who uses 1.12691×10^{-8} TW per person of energy), the world will need an astronomical 106 TW of energy in 2050, or for the world to live like a Canadian in 2050 will require even more energy (131 TW). Three entries, China, India, and Africa, are particularly pertinent to the world's energy future. These areas have low per capita energy use. However, because they possess the largest populations on our planet and because energy consumption scales directly with a country's gross domestic product (GDP), their energy use will only increase dramatically as they modernize.[2,3]

Extremely conservative estimates place the global power need to be 30 TW in 2050, even in light of unprecedented energy conservation.[2] To illustrate the extent of the required

Table 1. Global Energy Consumption for Selected Regions[a]

region	energy use (in TW) per person	population in 2007	energy use by region (in TW) for 2007	projected energy need (in TW)[b]
Africa	0.05333×10^{-8}	945 914 290	50.44×10^{-2}	5.0
Australia	0.98669×10^{-8}	20 749 630	20.47×10^{-2}	92.7
Brazil	0.17466×10^{-8}	193 918 580	33.87×10^{-2}	16.4
Canada	1.39603×10^{-8}	32 935 960	45.98×10^{-2}	131.2
Chile	0.23675×10^{-8}	16 303 850	3.859×10^{-2}	22.3
China	0.19680×10^{-8}	1 321 851 890	260.1×10^{-2}	18.5
Equatorial Guinea	0.32137×10^{-8}	599 760	19.27×10^{-2}	30.2
France	0.58804×10^{-8}	63 714 450	37.47×10^{-2}	55.3
Germany	0.57478×10^{-8}	82 401 000	47.36×10^{-2}	54.0
Iceland	2.21873×10^{-8}	301 930	0.6699×10^{-2}	208.6
India	0.05679×10^{-8}	1 124 134 800	63.84×10^{-2}	5.3
Italy	0.45795×10^{-8}	58 177 200	26.64×10^{-2}	43.0
Japan	0.58960×10^{-8}	127 433 490	75.13×10^{-2}	55.4
Malaysia	0.32478×10^{-8}	24 835 240	8.066×10^{-2}	30.5
Norway	1.38557×10^{-8}	4 627 930	6.412×10^{-2}	130.2
Russia	0.71784×10^{-8}	141 377 750	101.5×10^{-2}	67.5
Singapore	1.68346×10^{-8}	4 553 010	7.665×10^{-2}	158.2
Spain	0.55106×10^{-8}	40 448 190	22.29×10^{-2}	51.8
Sweden	0.83360×10^{-8}	9 031 090	7.528×10^{-2}	78.4
United Kingdom	0.52041×10^{-8}	60 776 240	31.63×10^{-2}	48.9
Turkey	0.19320×10^{-8}	74 767 840	14.45×10^{-2}	18.2
United States	1.12691×10^{-8}	301 290 330	339.5×10^{-2}	105.9

[a] Taken from http://www.eia.doe.gov/emeu/international/energyconsumption.html (accessed 14 January 2010). [b] For entire global population (9.4 billion) in year 2050 based on individual country's energy use in 2007.

conservation, consider the last column of Table 1. On average, the per capita energy use needed for a global population in 2050 will have to be the amount of energy a person uses today in Equatorial Guinea. Hence, for the legacy world to live as it does today, on the per capita energy use of an individual in Equatorial Guinea, strident technological and social advances will have to be made to ensure such energy conservation. And even in light of this energy conservation, an additional 16 TW of power will be needed owing to the growing population of the nonlegacy world.

To deliver an additional 16 TW to our world by 2050 is not a simple task. As has now been documented extensively in the literature, most energy sources are insufficient to keep pace with the growing global energy appetite.[2,4,6−8] Biomass is a limited energy supply owing to the low energy efficiency of photosynthesis.[9] Nuclear energy requires a large number of sites that will be difficult to build fast enough to keep up with energy demand.[7] Moreover, a heavy nuclear-based energy supply will not occur without widespread public acceptance,[10] and the energy density of wind is simply too low.[7,8] Whereas the fossil energy resource base is sufficient to satiate the future energy appetite, atmospheric CO_2 concentration will likely triple if the increased energy need in this century is met with coal, oil, and gas.[11] While the consequences of this increase in greenhouse gases (GHG) cannot precisely be predicted, there is little doubt that large ecosystems are being perturbed on an unprecedented scale. It is therefore imperative that the global community moves as quickly as possible to carbon-neutral energy sources.

Sunlight is the preeminent carbon-neutral energy source for the future. The terrestrial solar insolation resource base exceeds that of all other renewable energy sources combined,[12] and it additionally far exceeds what is necessary to support even the most technologically advanced society. The ability of solar to meet the global energy demand of the future is well documented.[2,6,12,13] However, a major challenge confronting the deployment of solar energy on a large scale is its storage. Because society relies on a continuous energy supply and solar energy is diurnal and also subject to intermittency arising from variable atmospheric conditions, an inexpensive storage mechanism is needed for solar energy to become a material contribution to the primary energy supply.

Solar energy storage has three major consequences for society:

(i) *A plentiful, large-scale energy supply by making solar available 24 h a day, 7 days a week.* Figure 1 shows a typical power demand curve of a utility company overlaid with a typical daily output from a 4.5 MW solar farm in northeast Arizona administered by Tuscon Electric Power.[14] The quasiperiodic sinusoidal demand curve[15,16] and solar insolation curve are mismatched.[17] Storage mechanisms effectively permit the solar supply to become synchronous with the demand curve. In the legacy world, the current supply of energy by solar is small and fluctuations in the grid can be levelized by hydrocarbon-based thermal generation. As solar becomes a greater contributing energy source, fluctuations of the energy supply can seriously compromise the stability of the grid and the quality of electricity derived from the grid. In meeting the more severe fluctuations engendered by a solar supply, noncarbon-based storage mechanisms will become increasingly important as concern over GHG emissions increase. A cost-effective storage mechanism also enables solar to be a highly distributed source of off-grid power, which is particularly relevant for the growth of the solar market in the nonlegacy world.

(ii) *The most secure energy supply.* Storage permits solar energy to be highly distributed and decentralized to the limit that the individual controls the energy on which she/he lives. Consequently, cyber or physical attacks on the energy infrastructure are effectively impossible. Moreover, solar energy storage has the potential to greatly enhance geopolitical stability. It is now well documented that greater economic security is accompanied by greater geopolitical

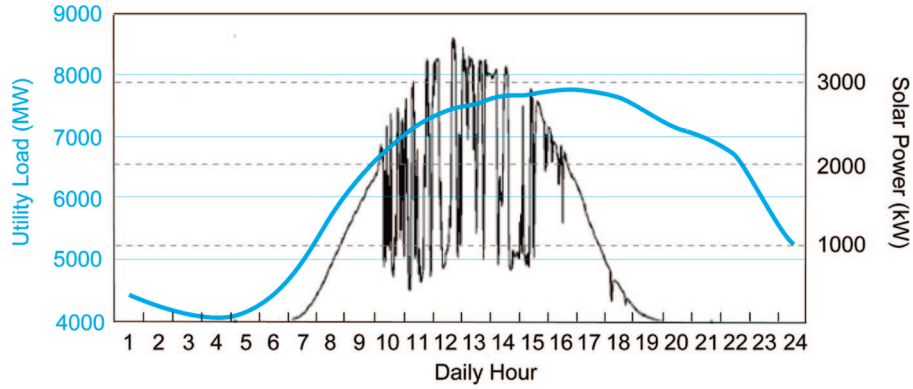

Figure 1. Utility load versus solar power output. Overlaid on the wind and demand curves is the power output (kW) sampled every minute for a 4.6 MW solar PV array in northeastern Arizona over the period of one day. Reprinted with permission from ref 14. Copyright 2008 John Wiley and Sons.

stability.[18,19] Because energy use scales with wealth, point-of-use solar energy will put individuals, in the smallest village in the nonlegacy world and in the largest city of the legacy world, on a more level playing field.

(iii) *The most direct way to reduce GHG emission in this century.* Acknowledging that it is the 6 billion nonlegacy users that are driving the enormous increase in energy demand by midcentury, solar energy systems at the individual level (personalized energy (PE))[20,21] may very well provide society its most direct path to a low-GHG future. The possibility of generating terawatts of carbon-free energy may be realized by making solar PE available to the 6 billion new energy users by high-throughput manufacturing. Because PE will be possible only if solar energy is a 24/7 available supply, a key enabler for personalized energy is small-scale and highly decentralized storage.

Thus, whereas storage is currently a weak link for the large-scale deployment of solar energy, its realization drives inextricably to the heart of a solution for society's energy challenge by addressing the triumvirate of a plentiful, secure, and carbon-neutral energy supply.

1.2. An Imperative for Discovery Research

Nonpracticing scientists and some technologists often mention that technologies for renewable energies exist, they simply need to taken off the shelf. This statement is partially true. One of the great triumphs of science over the past two decades is that it has established all aspects of renewable energy as a proven technology. A vast array of photomaterials have been created that can collect solar light efficiently. The harnessed solar light may be stored and released in any form that one desires, whether that be electrical, mechanical, or chemical. So then what is the research imperative? While every aspect of renewable energy is proven technology with no existent show-stopper, current options to harness and store solar energy are too expensive to be implemented. The imperative to science is to develop new materials, reactions, and processes that enable solar energy to be sufficiently inexpensive to penetrate global energy markets and especially in the nonlegacy world.

In addressing the foregoing imperative, it is important to realize that the design and development of inexpensive solar energy technologies for the legacy and nonlegacy worlds are at odds with each other. In the legacy world, energy systems of the past and present operate at large scale, they are

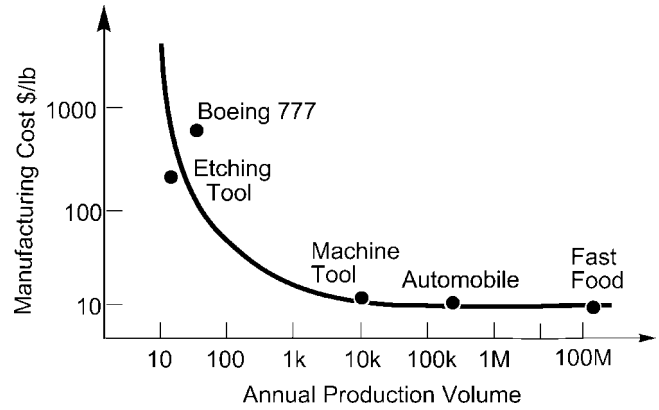

Figure 2. Manufacturing costs of consumer (non-hi-tech) goods as a function of weight and production volume. Data provided by Professors Martin A. Schmidt and Alexander H. Slocum (MIT). Reprinted with permission from ref 14. Copyright 2008 John Wiley and Sons.

centralized, and energy is distributed to the masses via an expensive and complex network. Such infrastructure is not viable in the near term future of the nonlegacy world, where it is cost prohibitive to build centralized energy and distribution systems. An alternative strategy that is better adapted to making energy available to the 6 billion new energy users is highly distributed energy systems for the individual.[20,21] This will require solar PE systems that can be produced by high-throughput manufacturing and that place a premium on low cost.

Low cost in a manufacturing environment is most profoundly affected by materials goods of the system (most generalized by the weight of the system) and the production volume.[22,23] This manufacturing issue is illustrated in Figure 2, which emphasizes consumer goods that are neither high-tech (i.e., pharmaceuticals, computer chips) nor commodity. The manufacturing of the goods shown in Figure 2 is the type that is needed for energy systems.[24] The figure is striking because manufactured goods that are very different in their weight, sophistication, and utility in our society, be it a fast food or airplane, fall on the same curve. One sees, to a first approximation, that the systems cost (cost of materials per their weight) will be low if it is able to be produced at a high volume. These criteria are precisely the antithesis of the design and production of most energy systems of the legacy world. Energy systems of the legacy world find their origins away from the asymptotic limit of Figure 2. Even if the materials cost per weight is at the limiting value of $10/lb, centralized energy systems are constructed at large scale

(i.e., large weight) and built one at a time. In 2007 in the U.S., the total value of generation, transmission, and distribution infrastructure for regulated electric utilities was $440 billion and capital expenditures exceeded $70 billion.[25] Reasonable recovery of capital expenditures requires design of energy systems that operate at large scale and high efficiency, and consequently energy systems of the legacy world come with significant balance-of-system (BOS) costs. Downscaling such technology is not economically viable because the BOS costs do not scale commensurately. Thus off-the-shelf technology and "existing" technologies will be difficult to adapt to low-cost energy systems. Rather, the disruptive energy technologies of the future will be those that conform to the message of the figure—light and highly manufacturable energy systems that are at the same time robust and require low maintenance. Simply put, new research is needed to provide our society with the "fast food" equivalent of energy systems.

1.3. Scope of Review

Solar energy technologies are moving toward a "fast food" energy model. Low-cost and large-scale manufacturing are already emerging trends in the capture and conversion of solar energy. Thin film,[26,27] ribbon,[28] "plastic" (i.e., polymer),[29−32] and nanoengineered[33] photovoltaics each have the promise of low cost because they can be adapted to high-throughput manufacturing. Indeed, in the case of thin film photovoltaics, low manufacturing cost owing to high volume production of cells that possess a minimal amount of semiconducting material has resulted in a multibillion dollar market.[34] Numerous reviews may be found on the burgeoning photovoltaic industry,[35,36] and thus this topic will not be treated here. Conversely, progress on developing inexpensive solar energy storage has been much slower. For this reason, the focus of this review will be solar storage technologies with an emphasis on solar fuels. In this area, there have been expansive reviews on molecular oxygen[37−40] and hydrogen[41,42] evolving catalysts, especially with regard to artificial photosynthesis and more generally photocatalysis.[43,44] However, for most of these systems, quantitative data that permits the performance of a given catalyst to be evaluated are unavailable. Specifically, the relation of activity (current density for electrochemical catalysts or turnover frequency for a molecular catalyst) as a function of overpotential, over a potential range (as opposed to a single point measurement), is a key parameter that permits a side-by-side evaluation of the efficacy of a catalyst to be ascertained.[45] To this end, this review will only include catalysts for which such data are provided. The preponderance of data that relates activity over a potential range is available for heterogeneous catalysts for which activity is evaluated electrochemically. Hence most cases presented herein will be for heterogeneous catalysts, although there are exceptional cases where activity data are provided for homogeneous catalysts. For the latter, the homogeneous catalysts are included and their performance is evaluated side-by-side with heterogeneous systems.

A comprehensive treatment of solar storage methods will be presented in this article. Two extremes of energy storage are large-scale and centralized storage (e.g., grid) versus small-scale and highly distributed. Within these two regimes, a variegated storage capacity is demanded for a solar resource.

Centralized stored energy technologies can make the grid more reliable and stable when fed by a solar resource and improve the efficiency of grid operations. An important report on grid energy storage in developed economies was prepared by the Electricity Advisory Committee of the U.S. Department of Energy in December 2008.[46] There are many different applications for centralized (grid) energy storage. Energy storage: (i) provides greater grid regulation and stabilization by mitigating short-term fluctuations (minutes to hours) and distortions arising from a solar supply, (ii) reduces the dependency on spinning reserves, which maintains excess generation held in readiness to meet failure or collapse of generating sources and transmission and distribution, (iii) permits load shifting by allowing surplus energy to be stored during periods of high solar generation and released at times of increased demand and when solar generation has ceased, (iv) facilitates peak shaving by permitting stored solar energy to be released over the minute to hour peaks in the demand curve.

Decentralized stored energy provides additional value for solar energy while retaining many of the foregoing benefits of centralized energy storage. Stored energy at or near the site of demand offers inherently higher service reliability than what could be offered with centralized energy storage owing to the nonlinear nature of transmission and distribution losses.[46] This is especially true for diurnal peak shaving because a high percentage of the transmission and distribution losses occur on distribution circuits.[46] Furthermore, small-scale, extremely distributed energy is likely to assume greater importance in the future, and it appears to be a necessity for the energy systems of the nonlegacy world where transmission and distribution hardware is prohibitively costly. For extremely distributed solar energy storage, a robust energy storage system is a necessity.

Different methods for stationary energy storage that are adapted to solar generation are summarized in Figure 3. These different technologies are of four forms: (i) potential energy (pumped-hydroelectric, compressed-air, electric charge in super/ultra capacitors), (ii) kinetic energy (flywheels), (iii) chemical energy (in the form of batteries or fuels), (iv) thermal energy (concentrated solar thermal, geothermal). A brief outline of the energy storage technologies described in this review is provided in Figure 3. These technologies are distinguished by the time scales on which energy is stored and their intrinsic power and energy densities. Figure 4[47,48] graphically illustrates the various time scales for some of these technologies, and Figure 5 provides a Ragone plot for the different storage technologies. In view of Figure 2, the issue of energy density is especially important to large-scale energy storage because cost is so intimately tied to the overall cost per weight of the storage technology. This review will therefore emphasize the chemistry of solar fuels because they have the highest energy density of any storage mechanism. Before proceeding to solar fuels chemistry, potential, kinetic, and thermal energy storage mechanisms will be reviewed. Although the discipline of chemistry has little or no role in these storage mechanisms, knowledge of other storage technologies is of value because they provide a benchmark for solar fuels research. We note that some recent reviews on nonfuels storage technologies have appeared[49−53] and thus they will only be briefly discussed here.

2. Large-Scale Centralized Energy Storage

Very large-scale energy storage at the utility level may be achieved with pumped hydroelectric storage (PHS) or compressed air energy storage (CAES). The feasibility of

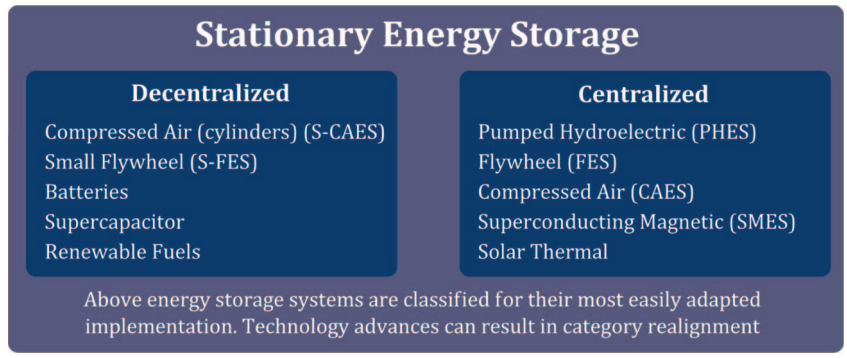

Figure 3. Summary of outline for different storage technologies described in this review.

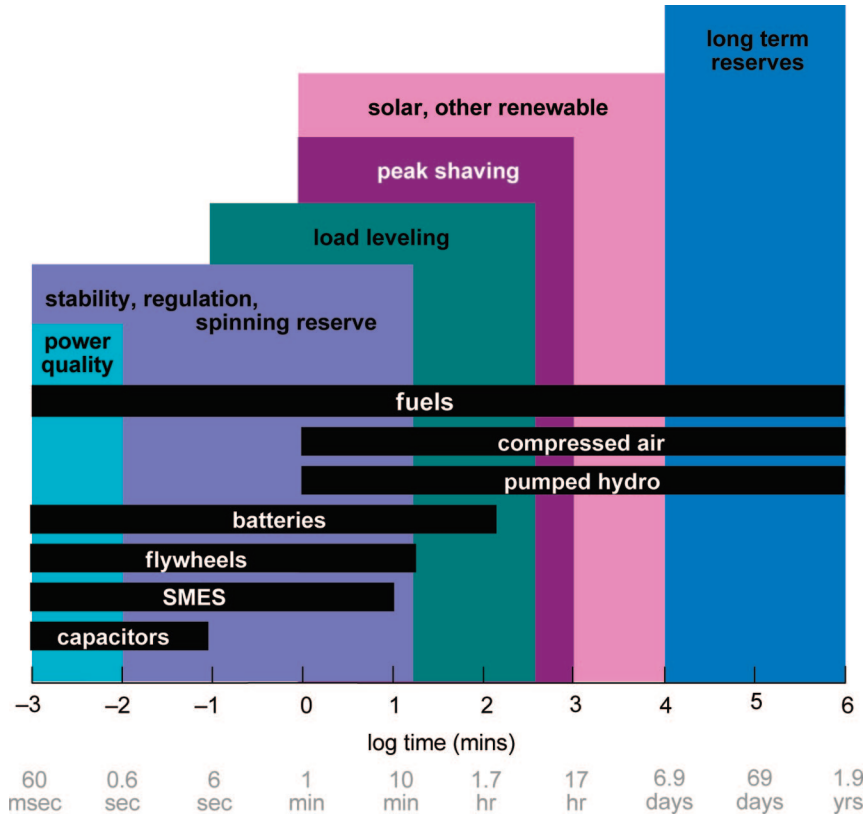

Figure 4. Characteristic time scales for energy storage applications and technologies. Times rounded to nearest time decades in minutes. Adapted from refs 47 and 48.

these methods for large-scale energy storage depends heavily on geography for their implementation and other factors such as public acceptance.

2.1. Pumped Hydroelectric Energy Storage (PHES)

Hydroelectric power generation is derived from the kinetic energy of falling or flowing water. There are 150 pumped storage facilities in the United States and approximately 280 installations worldwide. Hydroelectric energy generation, by a large margin, is the largest source of renewable energy in the United States,[54] although few such facilities have been built in recent decades. Worldwide, hydroelectricity accounted for 17.4% of total power production in 2005,[55] and in some countries, namely Norway (98.9%), Brazil (83.7%), and Venezuela (73.9%), hydroelectricity is the majority source,[56] a testament to the affordability, robustness, and scalability of hydropower, although this storage method is limited by geographic constraints.

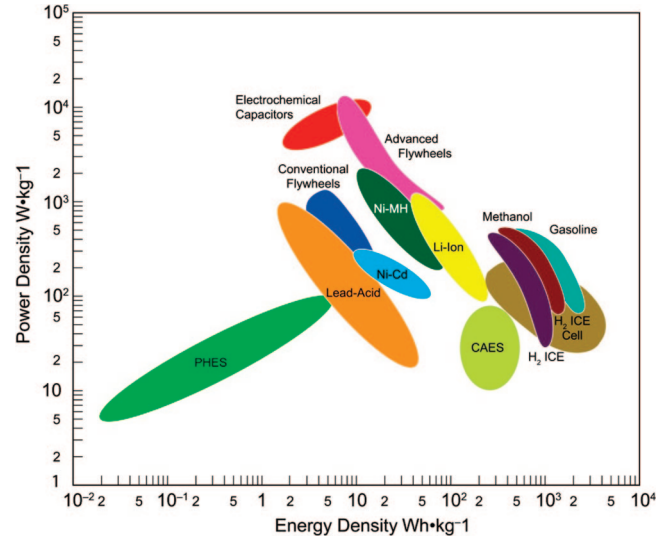

Figure 5. Ragone plot of specific power density versus energy density of various storage methods presented in this review.

A storage mechanism utilizing hydroelectric power generation may be realized if available surplus or off-peak generating capacity is used to pump water from a low-elevation reservoir to a reservoir at higher elevation. The stored energy is recovered by releasing the water for hydroelectric power generation. Modern pumped-hydroelectric energy storage (PHES) facilities routinely utilize reversible pump turbines, where the water pump and the turbine are a single, bidirectional device. The overall process can have a high round trip efficiency, but owing to the low energy density of a water column, large volumes of water are needed.

The maximum energy stored in elevated water, in joules, is simply the gravitational potential energy (E_p) of the water, given by

$$E_p = mgh \quad (1)$$

where m is the mass of the water in kg, g is the gravitational force constant, 9.8 $m \cdot s^{-2}$, and h is the height, or vertical displacement, of the water in meters. Thus, the maximum energy density of pumped water, or any fluid for that matter, is quite meager at 9.8 $J \cdot kg^{-1} \cdot m^{-1}$. The maximum power, P, in watts, delivered by a hydroelectric facility, is given by

$$P = \rho ghQ \quad (2)$$

where g and h are defined as before, ρ is the density in kg/m^3 of the fluid that drives the turbine, and Q is the flow in m^3/s.[57]

The expressions above for maximum energy storage and power delivery are of course idealized and do not take into account the efficiency of the device components. In a hydroelectric storage system, the chief sources of efficiency loss are friction, including the internal friction of the pump/turbine assembly, and water evaporation, estimated to occur at a rate of 4.5−7.6 gallon $kW\ h^{-1}$.[58] Cycle efficiencies for hydroelectric storage range from 63% to 80%,[59] scaling with the power rating of the pump, and in some cases, cycle efficiencies as high as 90% may be achieved under optimal operating conditions.[60−62] Using these numbers, it can be expected that approximately 50−70% of the electrical energy fed into a pumped storage device can be recovered for later use. Accounting for these losses, the maximum energy density for pumped water is realistically ∼5−7 $J\ kg^{-1}\ m^{-1}$.

Although of poor absolute energy density, PHS allows large quantities of stored energy to be readily converted to electricity. In terms of scale, hydroelectric power requires 50 km^2 per 100 MW.[58] The capacity of pumped-storage facilities ranges considerably, although power outputs of >1000 MW are not uncommon. Where the resources are available, small-scale hydroelectric facilities can be constructed, using flowing water from small streams to provide energy on the kW scale. On a small scale, the efficiency suffers relative to the large hydroelectric plants, with efficiency ratings of ∼50% being typical for micro (<100 kW) hydroelectric turbines.[63] Thus PHS appears to be optimal for large-scale energy storage applications, as accessed through the electric grid or in applications where the source of generation can be colocated with the PHS facility. These small-scale hydroelectric devices conventionally do not include PHS, which is untenable for small-scale and distributed energy storage.

In the case of centralized solar, sites needed for concentrated solar thermal power plants versus large water reservoirs are geographically incompatible. In response to this issue, the construction of underground reservoirs has been discussed,[64,65] where topological geographical restrictions are largely ameliorated. Upper and lower reservoirs can be placed proximate with a lower reservoir. Although the construction of underground PHS is technically feasible,[66] the cost of construction of such storage sites at such low energy density suggests that this storage mechanism for centralized solar energy will be unimportant as technical developments in alternative storage technologies such as concentrated solar thermal storage methods come to the fore.

2.2. Compressed Air Energy Storage (CAES)

Whereas compressed air has been utilized for centuries to provide mechanical work, more recently it has received increased attention as a means of storing electrical energy. In CAES, air is precompressed using the low-cost electricity from the power grid at off-peak times and utilizes the stored energy together with some gas fuel to generate electricity as needed. This storage technology has the potential to provide energy storage on very large scales. Compressed air energy storage (CAES) is primarily being targeted to store excess energy generated by wind farms[67] but in principle *could* be used to store excess electrical energy derived from any source including solar.

A gas will increase in temperature as it is compressed. With increasing temperature, the gas becomes resistant to further compression (i.e., each increment of compression must be performed on a volume of gas that is at higher pressure than if it had not been heated by prior compression). While undergoing expansion, the gas cools, resulting in a second inefficiency; at each increment of expansion (i.e., the gas is at lower pressure than if it had not been cooled by prior expansion), the expanding gas can do less useful work. The management of the heat during compression and expansion defines the different conditions (i.e., adiabatic, diabatic, or isothermal) under which CAES is performed. In an adiabatic cycle, the heat generated upon air compression is stored and returned to the air upon expansion, whereas the heat generated in diabatic storage is removed from the system. The air must be reheated (usually by natural gas for utility grade storage or by a heated metal mass for large uninterruptible power supply (UPS)) prior to expansion in the turbine to power a generator. Whereas the efficiency of a diabatic system is intrinsically much lower than an adiabatic system, the former is simpler to engineer and hence is less costly; consequently, it is the only system to be used commercially for CAES. Isothermal CAES has attracted interest for smaller compressed air storage using cylinders for gas storage. In isothermal systems, during sufficiently slow cycling, heat can flow out of the system to the surroundings during compression and into the system from the surroundings during compression. If the gas remains at the same temperature during both compression and expansion, then the heat recovered from the surroundings during expansion is equal to the heat originally emitted to the surroundings during compression.

The thermodynamics governing the theoretical energy storage density of compressed air is the amount of work (w) done when a gas changes its volume from V_i to V_f[68]

$$w = -\int_{V_i}^{V_f} p_{ex}\, dV \quad (3)$$

where p_{ex} is the external pressure of the system. The energy stored when a gas is compressed depends on whether

CAES is performed under adiabatic, diabatic, or isothermal conditions. The maximum energy storage in a compressed gas occurs when the gas is compressed reversibly and isothermally, and the external pressure, p_{ex}, is always equal to the pressure, p, of the confined gas and the temperature is constant. In this case, the solution to eq 3 yields

$$E_{max} = -nRT\ln\left(\frac{V_f}{V_i}\right) = -nRT\ln\left(\frac{P_f}{P_i}\right) \quad (4)$$

for the amount of theoretical energy contained in the compressed air. This idealized equation permits a discussion of maximum energy density. By using eq 4, an energy density of 114 kWh kg^{-1} is achieved when air, initially at standard temperature and pressure, is compressed to a pressure of 200 bar (~3000 psi). In practice, approaching the reversible limit for compression and expansion of gases requires very slow changes in volume; rapid compression of gas results in severe temperature changes and limits the energy storage efficiency. Factors such as the heat capacity of the gas, heat exchange in the system, and thermal equilibration also must be considered for more practical determinations of energy and power density.

Compressed air energy storage has been implemented as a hybrid generation/storage technology, and large amounts of energy storage can be realized. Coupled to power generation by conventional power plants or wind farms, a subterranean CAES system allows for storage of off-peak or excess power. The extra electricity is used to compress air into an underground cavern, such as a salt dome or depleted gas field. By using preexisting caverns with large volumes, costs associated with containment of the air are eliminated and adequate energy and power densities can be obtained without using unsafe temperatures or pressures. During peak hours, the compressed air is fed into a natural gas turbine, and the mixture is combusted to recover stored energy. Essentially, this mode of recovery allows the compression and expansion cycles of the combustion turbine to be decoupled, resulting in a 3-fold increase in the amount of turbine power per unit of natural gas.[50] It has been estimated that the turbine compressor stage uses 60% of the turbine's mechanical energy, and in a CAES system, this energy comes from the compressed air.[69] Operating pressures of 50−80 bar are typical, and a volume of 200−300 m^3 is required per stored MWh.[67] CAES systems successfully operating at >100 MW capacity have begun to appear, and several large CAES projects, with different storage media, are in development,[69,70] although long-term costs without research and development and demonstration support remain to be evaluated.

The drawbacks of large land areas, fortuitous geological features for large-scale CAES and a second carbon-based fuel source such as natural gas as an energy input during expansion can be mitigated for smaller scale CAES systems. To circumvent geologic constraints, air can be compressed in underground, high-pressure piping (20−100 bar), and at still smaller scales, air can be compressed and stored in high-pressure carbon reinforced gas cylinders. On these small scales, CAES may be managed isothermally, and the air can be coupled to an electric compressor that can be turned into a generator to deliver the power without the need for an external fuel input. Depending on recharging and discharging powers, the overall system efficiency can be well in excess of 50%. The cycle lifetime is limited primarily by the mechanical fatigue of the cylinders, and accordingly, cycling of 10^4 can be realized. Such smaller CAES applications are currently a topic of research and development.

3. Smaller Scale Grid and Distributed Energy Storage

3.1. Flywheel Energy Storage (FES)

Flywheels store energy in a rotating mass (called a rotor).[71,72] It is thus a kinetic energy storage mechanism. The rotating energy is transferred to the device (storage) and from the device (supply) as needed. The rotor resides in an evacuated or helium filled container to reduce aerodynamic losses and rotor stresses. For the storage of electrical energy, the flywheel is outfitted with an electrical machine and power electronic interface for conversion. The power interface includes the motor/generator, a variable-speed power electronics converter, and a power controller. Whereas the potential of flywheel energy storage (FES) systems to meet electrical energy demand response/load was recognized over a half-century ago,[72] market drivers, such as uninterruptible power supplies (UPS), are motivating development of FES as a key energy storing technology.

The potential energy that is stored in a rotating device, E_{rot}, is given by

$$E_{rot} = {}^1/_2 I\omega^2 \quad (5)$$

where I is the moment of inertia and ω is the rotational speed. The moment of inertia depends on the mass (m) and shape of the rotor. A commonly used configuration for a flywheel is one that concentrates the mass at the rim of radius R. For such a rotor, the moment of inertia is given by

$$I = mR^2 \quad (6)$$

Thus the energy stored in a rotating cylinder is ascertained by substituting eq 6 into eq 5 to give

$$E_{rot} = {}^1/_2 mR^2\omega^2 \quad (7)$$

FES thus increases with increasing mass of the rotor at increasing distance from the axis of rotation and increasing rotational velocity. The practical limitations on FES depend on strength of materials, whereas the efficiency depends on the energy extraction over different rotational speeds and loss of energy owing to friction. Taking into account these practical limitations, the tensile stress in the rim at angular speed, ω, is

$$\sigma_{max} = \rho mR^2\omega^2 \quad (8)$$

The maximum theoretical energy density of the exemplary flywheel described here is given by

$$\text{energy density} = {}^1/_2 m\sigma_{max}/\rho_m \quad (9)$$

σ_{max} is the allowable tensile strength and ρ_m is the density of the material. Consideration of this expression leads to the two classes of FES systems: conventional (i.e., low speed, 6000 rev min^{-1}) and advanced (i.e., high speed, 50 000 rev min^{-1}) FES. Conventional flywheels are composed of metals, which have high tensile strengths, but the density of these materials is large. This leads to the low energy density and moderate power density for flywheels shown in Figure 5.

Steel FES systems have specific energies of ~5 Wh kg^{-1}. Advanced FES systems employ glass-reinforced and carbon-reinforced polymer composites, which greatly reduce ρ_m and at the same time improves upon σ_{max} because the inertial loading which causes stress at high rotational speeds is minimized for lighter materials. Energy densities of ~100 Wh kg^{-1} have been achieved for composite rotors and flywheels using magnetic bearings (here, the flywheel is housed in a vacuum-sealed steel container and employs a high-speed magnetic lift system) to reduce energy losses due to friction. Future flywheel designs seek to incorporate high-temperature superconducting magnetic bearings,[73] which have a rotational drag more than 2 orders of magnitude lower than that of conventional magnetic bearings and several orders of magnitude lower than that of mechanical bearings.[74] However, the specific energy and specific power of the complete FES system may be reduced by at least a factor of 10 when the weight of the complete system, including containment, vacuum system, and electrical interface, is taken into account.

Because the rotor is fixed in a flywheel, energy may be stored by increasing the rotational velocity of the flywheel. Stored energy from the flywheel may be released upon decreasing the rotational velocity of the flywheel. Because the speed of a flywheel can be adjusted quickly (0.1 s),[74] flywheels can store and release energy at high rates (0.1 s-h) for many cycles (100 000−2 000 000) and with long service lives (15−25 years) and appreciable energy storage (0−1000 MW), thus making them attractive for stationary energy storage applications, the most important of which is UPS and power quality (PQ) systems. For such load management, flywheel systems of 1000 kWh of energy storage may be achieved with facility, and for smaller distributed energy storage, flywheels systems of 1−5 kWh are common. A drawback of flywheels is that they are manufactured with relatively high capital expenditure (capex) costs (for 1 MW, 0.25 MWh, total capex is $750 000−$2 000 000) and they have relatively high standing losses. Whereas the energy storage efficiency of FES can be intrinsically high for the most advanced flywheel energy storage systems (at high rotation speeds, the useful stored energy can approach 90% of E_{max}),[75] this efficiency decreases at low discharge rates, mainly as a function of the power electronics efficiency and when cycling is not continuous. When the power interface is switched off, self-discharge can be significant and the energy storage efficiency may be severely compromised owing to losses associated to the rotor (e.g., frictional losses, etc.). Consequently, FES storage efficiencies are generally rated in standby mode where the power interface is often switched on and off intermittently to maintain a constant speed of the rotor. Standby self-discharge rates are found to be in the range of 2% per h of rated energy content during steady-state rotation and are higher at lower speeds.[76]

These high self-discharge rates limit FES to short-term energy storage; they are better thought of as high- or surge-power devices for applications that involve the frequent charge and discharge of modest quantities of energy at high-power ratings (e.g., a typical FES device that stores 1 kWh of electricity may be charged−discharged at a rate of 25−50 kW).

Several applications exist for FES. Whereas FES is currently used for UPS systems, load following and peak power supply, telecommunications, power quality improvement, and rail support, FES research is now being explored as a storage mechanism for renewable energy (though mostly wind and not solar). Potential applications to renewable energy systems include (i) power smoothing, avoiding rapid voltage fluctuations, and flicker (continuous cycling), (ii) power system stability (high power cycling and injection), (iii) grid reinforcement (peak lopping, distributed storage), and (iv) bridging power until a diesel generator set in a hybrid stand-alone power system is started and ready to be brought online.

3.2. Superconducting Magnetic Energy Storage

Superconducting magnetic energy storage (SMES) is achieved by storing DC electricity in the cryogenically cooled coils (−270 °C) of the magnet. The SMES system is charged by elevating the current within the superconducting inductor with DC current, rectified from AC current. When needed, current is released from superconducting coils and reconverted into AC. Because there is nearly no power loss due to ohmic resistance in the coils, instantaneous efficiencies of SMES systems can be >90% for a charge−discharge cycle.[77,78]

The energy density of a magnetic field is

$$\text{energy density (SMES)} = \frac{1}{2}\mu H^2 \qquad (10)$$

where μ is the permeability of the storage medium and H is the strength of the magnetic field, which increases with current to limit of the critical current beyond which superconductivity is quenched. Practically, energy densities have been achieved with SMES that are 20× that of classical magnets.[79]

As opposed to batteries, SMES systems are capable of near total discharge of the stored energy and can be continuously operated over a large number of complete charge−discharge cycles on a fast millisecond response time (ms). Although original SMES design and installation targeted large-scale systems,[80] most installations of SMES are in the range of 280−830 MWh capacity with power outputs as high as 2.5 MW.[81] Although small in market penetration, where used, SMES systems have been used to provide transmission voltage support and power quality to customers in the United States, Japan, Europe, and South Africa. These units not only provide energy storage for short-term power quality issues but they can also be sized to provide load leveling and spinning reserve for longer periods of time. The major shortcoming of SMES is its high comparative cost owing to the need for low temperatures. Thus wider implementation of SMES is intrinsically tied to the discovery of high-temperature superconductors.

4. Chemical Energy Storage: Electrochemical

4.1. Batteries

Batteries are the most common electrochemical energy storage (EES) technology. Numerous battery technologies have reached the consumer market, and more are poised to reach consumer markets within the next decade. In a battery, electrons flow (in an external circuit) from one side of the device (the anode) to the other side of the device (a cathode). To maintain electroneutrality, cations must also flow in the same direction but along a separate path (within the electrolyte contained inside the battery cell) so that the battery

Table 2. Summary of Battery Technologies[a]

battery	anode	cathode	voltage (V)	energy density Wh·kg^{-1}[b]	cycle life
lead−acid	$Pb + SO_4^{2-} \rightarrow PbSO_4 + 2e^-$	$PbO_2 + 4\,H^+ + SO_4^{2-} + 2e^- \rightarrow PbSO_4 + 2H_2O$	2.1	35	800
nickel−alkaline	$M + 2OH^- \rightarrow M(OH)_2 + 2e^-$	$2NiO(OH) + 2H_2O + 2e^- \rightarrow 2Ni(OH)_2 + 2OH^-$			
	M = Cd		1.3	35	700−2000
	M = Zn		1.6	70−120	500
	M = Fe		1.4	30−50	3000
	or				
	$2MH + OH^- \rightarrow 2\,M + H_2O + 2e^-$		1.2	75	600−1000
	or				
	$H_2 + 2OH^- \rightarrow 2H_2O + 2e^-$		1.2	60	6000
lithium-ion	$LiC_6 \rightarrow Li^+ + e^-$	$MO_x + Li^+ + e^- \rightarrow LiMO_x$ (M = Co, Ni, Mn, V)	2.5−4.5	150	1200
high T-sodium	$2Na \rightarrow 2Na^+ + 2e^-$	$2Na^+ + 2e^- + xS \rightarrow Na_2S_x$	2.1	170	1800
		or			
		$2Na^+ + 2e^- + NiCl_2 \rightarrow Ni + 2NaCl$	2.6	115	
liquid flow	$Zn \rightarrow 2Zn^{2+} + 2e^-$	$Br_2 + 2e^- \rightarrow 2Br^-$	1.3		1000
	or	or			
	$V^{2+} \rightarrow V^{3+} + e^-$	$VO_2^+ + 2H^+ + e^- \rightarrow VO^{2+} + H_2O$	1.6	29	
metal−air	$Zn \rightarrow 2Zn^{2+} + 2e^-$	$O_2 + 2H_2O + 4e^- \rightarrow 4OH^-$	1.2	300	0

[a] Data taken from refs 87 and 88. [b] Theoretical limiting energy densities: lead−acid, 252; nickel−alkaline, 240−300; lithium-ion, 400; high T-sodium 750−790; metal−air, Li 13000, Cd 4600, Mg 6800, Al 8100, Zn 1300, Fe 1200 (note: these quoted energy densities do not correct for the weight of the metal oxide product at the cathode; when this is included, the energy densities of all of these metal air batteries is greatly reduced).

does not short circuit. The flow of electrons and cations during battery discharge permits devices to be externally powered. Energy storage is achieved by reversing the electron and cation flow by applying an external energy source. For solar energy storage, the sun may power a photovoltaic to drive the battery cell reactions in reverse. In this way, solar energy can be stored as electrochemical energy.

Batteries are low energy density storage devices (see Table 2 and Figure 5) with little room for improvement. In a battery, the electrons must reside on atoms within the anode and cathode. The volume in which the electron and attendant cation reside, and transfer is thus limited by the physical density of materials composing the cathode, anode, and electrolyte. Some of the lightest elements in the periodic table, and hence lowest physical densities, are already used as battery materials, and consequently energy densities of batteries have approached a ceiling. For instance, the promise of lithium-ion batteries derives directly from the fact that Li is the third lightest element in the periodic table. Hence its use as an ion in the battery leads directly to the increased energy density. Continuing along these lines, all-liquid batteries[82] and metal−air batteries (metals = zinc, magnesium, lithium)[83] have the highest theoretical energy density because of the reduction of oxygen from air at the cathode; notwithstanding, practical energy densities will be far less.[84]

With energy density largely constrained by the physical properties of battery materials, most advances in battery technologies have come in the power density and cycle lifetime of batteries. The power density is the rate at which energy can be extracted from the battery. Here, significant advances have been made in battery technology. Another major area of improvement in batteries has been cycle life, defined as the number of charge/discharge cycles that a battery can undergo until its power output at 80% depth of discharge has diminished to 20% of its initial value. In both cases, new architectural designs of the anode, cathode, and electrolyte, especially in the nanodomain, lead to increased power (not energy) densities and cycle lifetimes.[85]

Batteries as a solar energy storage medium have the great advantage of high conversion efficiencies (typical 80%) because electricity is stored directly. Table 2 lists the characteristics of various battery technologies that have received wide attention as possible candidates for the storage of renewable electricity.[86,87] The battery is described in terms of the cell reactions on discharge, the open circuit potential for a charged cell, and the maximum energy density based on the cell reactions and mass of active material. Solar energy storage is achieved by using sunlight to charge the cell, i.e., drive the cathode and anode reactions shown in Table 2 in reverse.

4.1.1. Lead−Acid Batteries

Lead−acid batteries are among the oldest commercialized batteries and they are the most common form of battery storage used today. Lead−acid batteries consist of a lead dioxide (PbO_2) cathode and metallic (Pb) lead anode bathed in concentrated (38%) sulfuric acid. The open circuit (maximum theoretical) voltage of a lead−acid battery is 2.1 V. In addition to this high cell voltage, lead−acid batteries are comparatively inexpensive ($0.15/Wh) and exhibit high stability. The primary limitation of lead−acid batteries arises from their low specific energy density (30−40 Wh kg^{-1}) owing to the high atomic weight of lead (207.19 g mol^{-1}) as well as the high weight of inactive battery components (containers, separators, terminals, etc.). The weight of inactive components serves to reduce theoretical energy density (170 Wh kg^{-1}) by over a factor of 4, and accordingly much effort in recent decades has been focused on reducing the weight of inactive components.[88,89]

Lead−acid batteries for utility applications such as peak shaving have been examined but poor life cycle characteristics with deep discharge[90] have made them economically

infeasible for widespread use in the utilities market. For the same reason, they have found limited use for distributed solar storage.

4.1.2. Alkaline Batteries

Alkaline batteries utilize a concentrated potassium hydroxide electrolyte. Under such highly alkaline conditions, many metal oxides are stable to corrosion, allowing for a diverse array of battery types. Each specific variant of the alkaline secondary battery has its unique advantages and shortcomings, but the general operating principles are common to them all.[89−91] The battery anode consists typically of a metal or metal hydride and the cathode consists of a metal oxide. Reduction of the metal oxide by the metal or metal hydride produces the electromotive force.

The most well-developed cathode material for alkaline secondary batteries is the nickel oxide cathode. The Ni atoms in the oxide reside predominantly in the 3+ oxidation state and reduction from Ni^{III} to Ni^{II} takes place during discharge. Coupling this Ni oxide cathode with various metal anodes produces the common types of alkaline secondary batteries. For instance, combining a cadmium metal anode with the Ni oxide cathode produces the common nickel−cadmium battery. Similarly, utilizing a hydride intercalated Ni metal anode with the Ni oxide cathode produce the popular Ni metal hydride battery. Less common variants involve combining the Ni oxide cathode with a Fe metal anode (Ni−Fe battery) or a Zn metal anode (Ni−Zn battery). The complication of oxygen evolution during cell recharge (at 80%) requires that oxygen pressures be managed in either sealed or vented device configurations.

Among the Ni oxide based batteries, the most cost-effective are the Ni−Fe and Ni−Zn batteries ($0.15/Wh to $0.20/Wh). These batteries have not seen widespread use due to several drawbacks. In the case of Ni−Zn, the Zn cathode has a tendency to change shape and lose capacity over repetitive cycling. Additionally, upon recharging, Zn metal dendrites tend to form on the anode, leading to internal short-circuiting. The typical cycle life of Ni−Zn battery is only ∼500. In the case of Fe−Ni batteries, the primary shortcoming is the catalytic activity of the Fe electrode for hydrogen production. This typically limits the Faradaic energy efficiency to 30%.

More expensive variants of Ni oxide based batteries are the Ni−Cd ($0.40/Wh to $0.80/Wh) and Ni−metal hydride ($0.25/Wh) batteries. Despite the added cost, the Ni−Cd batteries are the second most widely used secondary battery in industry (after lead−acid) due to their low-temperature performance, high discharge rates, and long life. However, the relatively low natural abundance of Cd and its high toxicity has forced a slow replacement of these batteries with Ni−metal hydride (Ni−MH) or lithium-ion batteries. In the case of Ni−MH batteries, the Ni metal comprises the anode but does not participate in a redox reaction. The Ni reversibly uptakes hydrogen in the form of a metal hydride, and for this reason, the anode could be composed of any material that can reversibly uptake hydrogen. Research efforts have focused on developing alloys with higher hydrogen storage capacity. The specific energy density of Ni−MH batteries is approximately twice that of lead−acid or Ni−Cd batteries (Table 2), engendering their application in hybrid electric vehicles (e.g., Toyota Prius).

The Ni−hydrogen battery was developed for space applications. It couples a hydrogen fuel cell anode with a NiOOH cathode. These batteries have the highest performance ratings of Ni-based batteries, but they are expensive to construct because they require pressure containment of the hydrogen.

4.1.3. Lithium-Ion Batteries

The lithium-ion battery has reached mass market production owing to their emergence as the battery of choice in the portable electronics market. This battery technology employs a lithium intercalated graphite anode and metal oxide or metal phosphate cathode. The lithium intercalated graphite consists essentially of Li^+ and polyanionic graphite. Battery discharge entails electron transfer through the external circuit from the reduced graphite to the metal oxide/phosphate cathode. To preserve charge balance, this electron flow is accompanied by deintercalation of lithium ions at the anode and intercalation of lithium ions within the layered structure of the metal oxide or metal phosphate. Because of the low atomic weight of lithium and its low redox potential, the open circuit potential of the lithium-ion battery is ∼3.6 V. This is a 3-fold improvement relative to nickel alkaline cells and translates into a higher energy density (Table 2).[89,90,92] Numerous research efforts are being undertaken to enhance the efficiency of Li ion batteries.[88] One focus is on developing safe and reliable methods to replacing the lithium−graphite anode with a lighter lithium−metal electrode to increase the energy density. This would lead to an increase in energy density. Additionally, efforts are directed at improving the battery cathode. In particular, new materials with greater capacity for lithium intercalation are being explored. Another challenge in Li ion technology is to prevent reactions of the cycled Li electrode with the nonaqueous electrolyte. Such reactions result in catastrophic failures, which present a formidable challenge to the growth of this technology. New electrolytes (e.g., polymers, ionic liquids) are currently under investigation with the aim of overcoming this obstacle. The ability of lithium-ion batteries to economically serve electric utility applications has not yet been demonstrated except for some ancillary services provisions to some independent system operators.

4.1.4. High-Temperature Sodium Batteries

The use of batteries for energy storage for portable consumer electronics places a premium on batteries that operate at ambient temperature. However, for large-scale solar energy storage, this temperature restriction may not be paramount. Two main types of high-temperature batteries have penetrated commercial energy storage markets.

The sodium−sulfur battery employs liquid sodium for the anode and a molten S and Na_2S_x mixture for the cathode. The battery operates by the migration of sodium ions from the anode through a ceramic membrane to the cathode, where it reacts with sulfur to form sodium polysulfide. The battery operates at temperatures in excess of 300 °C. The energy density is high for a battery (200 Wh kg^{-1}). Because of the highly corrosive nature of sodium polysulfide along with the highly reactive nature of sodium metal, NaS batteries are difficult to engineer.

An easier to engineer high-temperature battery is the sodium−metal chloride battery. Here, sodium metal is again used as the anode, but the cathode consists of $NaAlCl_4$ impregnated in porous $Ni/NiCl_2$. During discharge sodium metal reduces the transition metal chloride to generate

metallic nickel with NaCl as a byproduct. This battery design typically operates at >200 °C and possesses an energy density of ~100 Wh kg^{-1}.[89,92]

High-temperature sodium batteries are used for energy storage by utility companies. Systems with cumulative energy-storage capacity of several hundred MWh have been manufactured and placed into operation in Japan; energy efficiencies are maintained in excess of 80% over 2500 cycles, lending this battery system for load-leveling applications. These devices have been found to be able to cycle on a daily basis, with charge/discharge durations up to eight hours per day, and with useful operating lives approaching 10 years. Moreover, because Na/S batteries can be discharged rapidly at five times base-load rates for short periods of up to 10 s, they can also be employed in power quality applications. The success of high T-sodium battery technology in Japan is largely a result of the relatively high price of electricity; there is a much smaller market penetration in the U.S. for high-temperature sodium batteries for energy storage applications.[89,93]

4.1.5. Liquid Flow Batteries

An attractive method for enhancing energy density is to involve a gaseous or liquid fuel in one or both of the electrochemical half reactions. Flow battery technology utilizes an active element in a liquid electrolyte that is pumped through a membrane similar to a fuel cell to produce an electrical current. Pumping in one direction produces power from the battery, and reversing the flow with an external energy supply (such as that provided by a renewable source) charges the system.

A typical liquid flow battery configuration comprises a two-electrolyte system in which bromine is coupled to zinc (ZnBr), sodium (NaBr), and vanadium (VBr) or a polysulfide. Other flow batteries rely on the presence of vanadium in sulfuric acid in different redox states. Two separate electrolyte-circulation loops are driven from separate storage tanks; the two electrochemical cells are separated by a membrane that allows the passage of one species of ion only. In the metal−bromine flow battery, an external tank containing bromine in an electrolyte solution is continuously flowed across the cathode. The electrochemical reaction through a membrane in the cell can be reversed (charge−discharge). The capacity of metal−bromine battery will scale with the size of the bromine fuel tank that is used. Large quantities of energy can be stored by using large reservoirs and a large number of cells. The advantage of this approach is that the storage capacity is not fixed by the cell dimensions but by the size of the electrolyte reservoirs. Because no solids are involved in the reactions, no volume changes occur during charging and discharging and, hence, cycle lifetimes are very long, especially compared to lead/acid technology, the technology most commonly used in these applications. Experimental metal−bromine batteries have been tested in all electric vehicles, and modules with 85 Wh kg^{-1} storage density have been produced;[89,94] large-scale projects for bromine−polysulfide flow cell have been implemented, and the battery is being considered for load leveling in the electrical supply industry.

4.1.6. Metal−Air Batteries

Even greater gains in energy density may be garnered if the anode and/or cathode reaction involves a gas. This method has been utilized most effectively in the zinc−air battery, which is a variant of the zinc−bromine battery in that liquid bromine is replaced by oxygen. The electrochemical reaction at the cathode is the four electron reduction of oxygen gas to water by zinc metal. Other metals including lithium and aluminum are also popular cathodes in a metal−air battery configuration. Because of the use of atmospheric oxygen for the cathodic half reaction, weight related to the cathode reactant is reduced and, consequently, metal−air batteries have higher theoretical specific energy densities. We note, however, that the increase in energy density of metal−air batteries is often embellished when practical limits are taken into consideration.[84] For instance, the specific energy of metal−air batteries is often referenced to the graphite electrode where the weight of air and the oxide formed at the cathode is not taken into account. When this is done, a more realistic and much lower energy density is obtained.[95]

A major drawback of metal−air batteries is that they cannot be cycled because the anode reaction upon discharge cannot be reversed. Instead, recharging the battery entails replacing the electrolyte slurry and installing a fresh metallic electrode. The inability to cycle the cell has led to investigations of both mechanically and electrically rechargeable metal−air batteries,[89] especially involving zinc,[96] but a viable rechargeable metal−air battery for storage has yet to be realized. Rechargeable metal−air batteries that are under development have a life of only a few hundred cycles and an efficiency of about 50%.

4.2. Capacitors

Electrochemical capacitors (ECs), often referred to as supercapacitors or ultracapacitors, store energy in the form of an electric field generated by the separation of electric charge between two electrodes. Unlike batteries, which store charge in a chemical reaction at its electrodes, ECs store electrical charge physically, without a chemical reaction taking place. In a conventional capacitor, the charge is stored on metallic sheets separated by a dielectric membrane. In ECs, the dielectric is replaced by an electrolyte and ion movement occurs within the electrode−electrolyte interface that possesses a very high surface area.[97,98] The practical difference between capacitors and ECs is a factor of $>10^3$ storage capacity for the latter.[99,100] Nevertheless, the overall energy density of ECs is still low, although recent advances regarding ion adsorption in microporous carbon on nanometer length scales have led to improvements in the energy density of supercapacitors.[101] The benefits engendered from ECs arise in power density. Because the charge is stored physically, with no chemical or phase changes taking place, the discharge−charge process is highly reversible and efficient, can be repeated tens of thousands of times, and is extremely fast, thus leading to the high power densities.[102] For commercially available ECs, the average cost per Wh is $10−20, nearly 10 times the cost per Wh for the best lithium−ion batteries. However, owing to the much greater specific power (5−10 kW kg^{-1}) as compared to ion batteries, the cost per kW is less, $25−50 per kW for ECs versus $75−100 per kW for Li-ion batteries. The stored energy in ECs discharges at ~5% per day, and thus stored energy must be used over short durations. The benefit of the ECs is that stored energy is available in ms time scales, and thus ECs can be useful for voltage regulation, frequency control, and other power quality applications. Other applications for ECs

include the portable electronic device market and low-emission hybrid cars, buses, and trucks.[103]

5. Chemical Energy Storage: Solar Fuels

Chemical fuels are a sustainable solution to small-scale, distributed energy storage. Fuels achieve high energy densities through the storage of electrons in the small volume of a two-electron bond between light elements (i.e., C−H, N−H, and H−H bonds). In comparing the energy densities of hydrocarbon (C−H based), nitrogen (N−H based), and hydrogen (H_2) fuels as a function of weight and volume, a few key points emerge: (1) hydrogen (H_2) has the largest energy density by mass (143 MJ kg) but suffers in volumetric energy density because it is a gas, (2) nitrogen-based fuels have modestly high energy content by mass and volume, and (3) hydrocarbon fuels provide the optimum energy supply in terms of volumetric energy density. This latter point, along with the economic availability of fossil fuels, provides the basis for the choice of hydrocarbon-based fuels as the energy currency of modern society. The challenge currently facing our society is to shift our view of chemical fuels from that of a carbon-based energy *source* to that of a form of (renewable) energy *storage*.

5.1. Solar Fuels in Nature

Photosynthesis has produced most of the energy that sustains life on our planet. It does so by storing solar energy in the rearranged bonds of water and carbon dioxide to oxygen and carbohydrate. Analysis of the energetics of the solar fuels conversion process shows that it is water splitting and not carbohydrate production that is at the heart of solar energy storage. The reversible potential for the water splitting reaction is,

$$H_2O \rightarrow H_2 + {}^1/_2O_2 \quad V_{rev} = 1.23\ V \qquad (11)$$

whereas the reversible potential for production of carbohydrate from water and CO_2 is

$$CO_2 + H_2O \rightarrow C_6H_{12}O_6 + O_2 \quad V_{rev} = 1.24\ V \qquad (12)$$

Note that water splitting is subsumed by reaction 12. On an electron equivalency basis, therefore, the production of the carbohydrate stores only 0.01 eV more energy than water splitting. Thus, the solar energy storage in photosynthesis is achieved by water splitting; the carbohydrate is nature's method of storing the hydrogen released from the water splitting reaction.

5.2. Artificial Photosynthesis and General Considerations of Water Splitting

Following the lead of nature, it is the water splitting reaction that lies at the nexus of any carbon-neutral solar fuels process. The first step of water splitting is the most difficult. Four O−H bonds of two water molecules must be broken with the concomitant formation of an O−O double bond. The four protons and four electrons that are released from this initial chemical transformation may subsequently be combined to form hydrogen, or as in photosynthesis, they could be combined with CO_2 to produce a liquid alcohol or hydrocarbon fuel. Recombination of the reduced fuel with O_2 regenerates the original species, closing the solar light-to-fuels cycle in a carbon-neutral fashion.

To this end, any effort to capture the photosynthetic process artificially must begin with water splitting. The overall transformation is a four-electron process that must be coupled to protons. The importance of proton-coupled multielectron transfer (PCmET) can be illustrated with the simplest reaction in chemistry, the reduction of two protons by two electrons to produce hydrogen. If the electron is uncoupled from the proton, and the proton is reduced by a single electron, then a H$^\bullet$ radical is produced at an energy cost of 2.3 V vs NHE. The addition of the second electron and second proton yields H_2 and the release of 2.3 V. Thus, the thermoneutral reaction for H_2 production confronts the sizable kinetic barrier of 2.3 V if the proton is not coupled to the electron and the reaction is confined to one electron steps. The first step of water splitting, to produce O_2 and four electrons and four protons, is significantly more complicated than hydrogen production. Not only is the proton and electron currency four (vs two for H_2 production), but the reaction is driven only at highly oxidizing potentials,

$$O_2 + 4e^- + 4H^+ \leftrightarrow 2H_2O$$
$$E_{anodic} = 1.23\ V - 0.059(pH)\ V(NHE) \qquad (13)$$

When coupled to hydrogen production

$$4e^- + 4H^+ \leftrightarrow 2H_2$$
$$E_{cathodic} = 0\ V - 0.059(pH)\ V(NHE) \qquad (14)$$

eqs 13 and 14 account for the ability to store 237.178 kJ mol^{-1} for water splitting (at 25 °C and 1 bar).

There are three general approaches to executing the water splitting reaction of eq 11 via half reactions (eqs 13 and 14). All require catalysts to lower the energetic requirements for producing hydrogen and oxygen from water with a solar input at a meaningful rate. Solar thermal methods use heat generated from solar light to decompose an oxide of a catalyst to oxygen. The reduced catalyst is subsequently coupled to hydrogen generation by its reaction with water to regenerate the oxide. Solar thermal methods to effect water splitting are outside the scope of this review. The two other approaches to promoting eq 11 are more authentic approximations of photosynthesis; they rely on coupling the water splitting catalysts to a light collection and solar-driven charge separation system. In the *indirect* solar fuels conversion approach, the spatially separated electron−hole pairs provided by a photovoltaic cell are channeled through a metallic conductor wired to electrodes that are modified by the catalysts. In the *direct* solar fuels conversion approach, the catalysts are integrated with a semiconductor and they capture the photogenerated electron−hole pairs directly. The tightly integrated direct approach is the one that Nature uses in photosynthesis and serves as the most faithful model for the artificial photosynthetic systems. For either the indirect or direct solar fuels conversion processes, the catalysts capture the electron−hole charge separated pairs and use them to mediate the PCmET reactions needed for efficient water splitting. The indirect solar conversion to solar fuels process couples the catalyst to an electrode, whereas the direct process couples the catalyst to a photoelectrode. To isolate the key aspects of catalysis from the charge separation and conversion processes occurring within semiconductors, the discussion below is focused on water splitting on metallically conductive electrodes. Recent strides have been

made in coupling water splitting catalysts to photoelectrodes,[104−106] but that topic is beyond the scope of this review.

The reversible potential difference caps the energy stored in eq 11 and excess applied voltage is lost as heat. However, to conduct water splitting at a practical rate, voltages in excess of the thermodynamic value must be applied. Indeed, the effective operational photovoltage V_{op} can be described by:

$$V_{on} = E_{rev} + \eta_a + |\eta_c| + \eta_\Omega \quad (15)$$

where η_Ω represents the voltage required to surmount resistance losses in the cell (e.g., solution resistance and contact resistance of the catalyst with the electrode, and η_a and η_c represent the overpotentials required to overcome the kinetic barriers inherent to half-reactions 13 and 14, respectively. To the extent that the magnitude of these overpotentials can be reduced by catalysts, the operational voltage will approach the reversible potential for water splitting and the efficiency of the overall process will be improved. In this context, a central challenge for chemistry is to develop improved catalysts for eqs 13 and 14 such that η_a and $|\eta_c|$ are minimized.

The anodic and cathodic overpotentials arise from the intrinsic activation barrier for the electrochemical half-reaction occurring at the electrode−solution interface (activation overpotential) in addition to limitations on the mass transport of reactant or products to or from the electrode. Whereas the impact of mass-transport limitations can be minimized through judicious cell design, the activation overpotentials are intrinsic properties of the catalysts utilized in the anode and cathode. This overpotential is logarithmically related to the current density (j) as given by the Tafel law:[107,108]

$$\eta = a + b \log(j) \quad (16)$$

where parameters a and b relate to the activity of the electrode and the mechanism of the electrode reaction, respectively. Extrapolating this linear relationship to $\eta = 0$ yields the exchange current density (j_0), which characterizes the intrinsic activity of the electrode under equilibrium conditions.[109] While j_0 is a useful metric for comparing different catalysts, an electrode material must possess a high j_0 in addition to a low Tafel slope (b) in order to be useful at the operational current densities required for a given energy storage application. Importantly, the logarithmic relationship between current density (catalyst activity) and overpotential means that quantization of one parameter without the other is of little value in evaluating a catalyst's performance. Accordingly, the ideal method of reporting catalytic activity is via a plot of steady-state current densities at a variety of overpotentials (Tafel plot).[109]

Virtually any current can be obtained with any catalyst material if a sufficiently large electrode is used. For this reason, it is common practice to normalize current densities to geometric surface area. Even with this normalization, the performance of an electrode will depend greatly on the 3-D nature (e.g., surface roughness) of the substrate or catalyst employed. Indeed, the preparation of high surface area substrates or catalysts is a common method of enhancing performance. While this issue complicates accurate comparisons of catalytic efficiency, the current density normalized to geometric surface area provides the metric of greatest relevance to electrode performance.

Whereas the efficiency considerations discussed above provide the primary motivation for developing new catalysts, they are not the sole figure of merit for solar fuels production. An ideal solar fuels catalyst should possess a number of other qualities including: (i) The ability to operate at high current densities at modest overpotentials over a wide range of pH values and electrolyte compositions, (ii) stability on the time scale of years to decades, (iii) a composition consisting entirely of earth-abundant materials, and (iv) a low-cost method of preparation and manufacturing. In practice, a single catalyst may never possess the best figure of merit in each of these categories and therefore the development of future solar fuels technologies will rely on choosing the right catalyst material for the particular application. In some cases, (e.g., highly distributed for nonlegacy societies), cost may trump efficiency as the crucial determinant. Therefore, it is the task of basic research to develop a wide of array of catalysts with diverse properties that will enable the development of next generation energy storage systems.

Research into new catalysts to promote eqs 13 and 14 can be broadly binned into two categories: molecular catalysts and extended solids. Although the latter has been studied more extensively over the last century, research of the former area has been flourishing in recent decades. Nevertheless, as of now, advances in molecular catalysts have yet to produce catalysts displaying activities comparable to those of extended solids. More problematic, new molecular catalysts are not assessed on a level playing field with the performance of solid-state catalysts. Because molecular science is turning to the energy problem with increasing rigor, it is important to understand the benchmarks against which advances will be made. In the following sections, a comparison of selected molecular and extended solid-state catalysts within the context of eqs 13 and 14 will be presented. We acknowledge that it is difficult to disentangle performance from geometric surface area because the active area is ill-defined in most studies. In performing comparisons of catalyst performance in the following sections, Tafel polarization data or single-point steady-state polarization data for surface immobilized molecular systems will be utilized depending on which is provided in the cited primary literature.

5.3. Catalysts for the Oxygen Evolution Reaction (OER)

5.3.1. Extended Solid-State OER Catalysts

The promotion of the oxygen evolution reaction (OER) by transition metal dioxides, spinels, and perovskites has been studied extensively.[110−113] Metal electrodes have also been examined, although it is now generally believed that surface oxides form on these metals prior to oxygen evolution.[114−116] The mechanism of OER is very sensitive to oxide surface structure, and therefore compositionally identically oxides may give rise to disparate electrokinetic profiles, depending on the thickness and morphology of the oxide layer and its method of preparation. Despite this, a generalized pathway for the OER on oxides proposes water coordination to a surface active site, with concomitant proton transfer to solvent and electron transfer to the electrode to form a surface M−OH species,[117]

$$M + H_2O \rightarrow MOH + H^+ + e^- \quad (17)$$

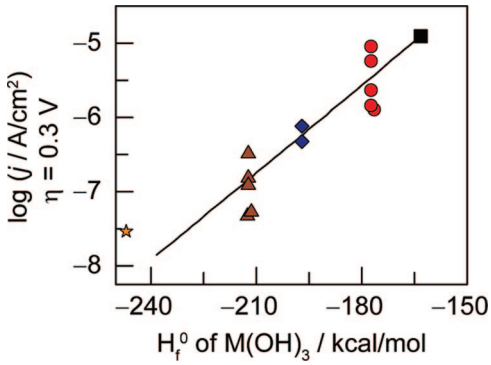

Figure 6. Steady-state OER current density, based on real surface area, at 0.3 V overpotential for Cr (orange star), Mn (green triangles), Fe (blue diamonds), Co (red circles), and Ni (black square) perovskites versus the corresponding enthalpy of formation for $M(OH)_3$. Reprinted with permission from ref 120. Copyright 1984 ECS—The Electrochemical Society.

A M−O species is presumed to form either via proton-coupled oxidation of the active site or disproportionation of two MOH species,

$$MOH \rightarrow MO + H^+ + e^- \quad (18)$$

$$2MOH \rightarrow MO + M + H_2O \quad (19)$$

The M−O species is proposed to decompose bimolecularly or is subject to attack by water (or hydroxide) to liberate O_2.

$$2MO \rightarrow 2M + O_2 \quad (20)$$

$$MO + H_2O \rightarrow M + O_2 + 2H^+ + 2e^- \quad (21)$$

Drawing on the rapid improvement of computational power in recent years, ab initio methods have been applied to compute $M-OH_x$ interaction energies on metal surfaces.[118] These studies conclude that oxygen evolution is only favored at high coverages of OH_x species, consistent with the experimental observation that surface oxide formation precedes O_2 evolution. While eqs 17−21 provide a framework for the OER on metal oxides, numerous alternative pathways have been proposed for specific classes of materials. And as is typical of solid-state catalysis, the detailed mechanism for the reaction is ill-defined, thus hindering a rational approach to developing better catalysts.

Despite this lack of mechanistic insight and consensus regarding the precise pathway operative for the OER, all proposals for the reaction invoke one or more $M-OH_x$ intermediates. Accordingly, the M−O bond strength may be expected to correlate with the metal oxide's electrocatalytic activity for the OER. Indeed, Bockris has shown that a strong correlation does exist in the case of first-row transition metal perovskites.[119,120] When the activity of a given perovskite is plotted versus the standard enthalpy of formation of the corresponding $M(OH)_3$ compound, a linear relationship is observed (Figure 6). Late transition metals (e.g., Ni and Co), which exhibit low enthalpies of formation for $M(OH)_3$, exhibit several orders of magnitude greater activity at the same overpotential relative to early metals (e.g., Cr) which exhibit high enthalpies of formation for $M(OH)_3$. This trend is rationalized by assuming that the enthalpy of formation of $M(OH)_3$ is directly proportional to the M−O bond strength of the catalytic intermediate participating in the rate limiting step. The observed inverse relationship between enthalpy of

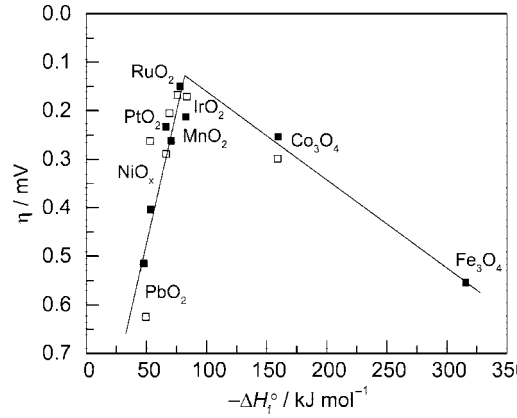

Figure 7. Volcano plot showing activity for O_2 production on metal oxide surfaces versus the enthalpy of transition of the oxide in acidic (■) and basic (□) solution. Overpotential measured relative to 0.1 mA cm^{-2} current density. Reprinted with permission from ref 121. Copyright 1984 Elsevier.

formation of $M(OH)_3$ and activity argues for a rate-limiting step involving M−O bond cleavage. Notably, this linear free energy relationship does not exhibit a peak common to the volcano plot relationship observed for hydrogen production on metals (section 5.5.1), and for this reason, the ideal M−O bond strength remains uncertain and oxides (particularly mixed metal oxides) possessing even weaker M−O bonds may exhibit higher activities.

While M−O bond strength appears to correlate well with activity for the first-row transition metal perovskites, alternative free-energy correlations for the OER have been proposed for oxides based on other physical properties such as the heat of transition between lower and higher oxide (Figure 7)[121] or potential matching between the O_2/H_2O couple and redox transitions in the oxide.[122] Computational studies[123] of adsorbate interactions on the 110 faces of IrO_2, RuO_2, and TiO_2 crystals provide evidence in favor the volcano-type relationships such as those shown in Figure 7.[121] However, a consensus on predictive parameters of OER activity has not been reached owing to a paucity of reliable catalyst performance data that rigorously account for surface area, surface defect, bulk defect, and conductivity effects.

The OER activity of numerous mixed metal oxides, in particular those of the spinels of the general formula $(M')_x(M'')_{3-x}O_4$, has been examined in hopes of exploiting synergistic M′−M″ activity relative to each of the pure metal oxide.[110,111] The activities of mixed Co−Ni oxides, scaled to their Brunauer−Emmett−Teller (BET) surface areas, have been evaluated as a function of the mole fraction of Co (Figure 8).[124] Maximum activity is observed for oxides with a Ni:Co ratio of 1:2, and this activity is double of that of a pure Ni spinel. The enhanced activity has been ascribed to changes in the lower/higher oxide transition energies[121] and the oxide work function upon metal atom substitution,[110] but the exact origin of the enhancement remains a subject of debate. Synergistic effects have also been observed for mixed-metal oxides of Ni−Cu,[125] Co−Mo,[126] Fe−Mo,[127] Cu−Co,[128] and Co−Cr−Fe,[129] among others.

The OER does not take place on a bare metal surface and, therefore, the conductivity of the material becomes a key additional consideration. The high number of defects in most oxides together with the high cation valency induced upon positive potential bias makes the ohmic penalties rather small.[113] Nonohmic barriers to electron transfer through oxide films have been shown to complicate the interpretation of

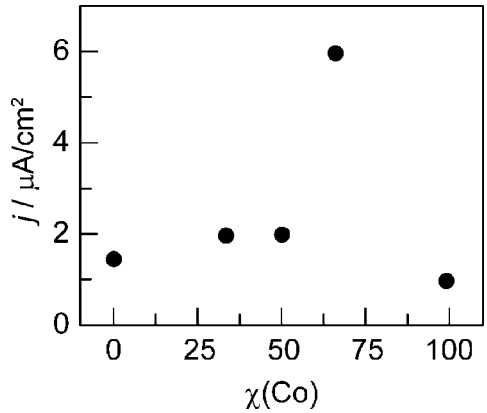

Figure 8. Steady-state OER current density, based on BET surface area, at 0.37 V overpotential as a function of the metal atom mole fraction of Co in Ni−Co mixed spinels. Reprinted with permission from ref 124. Copyright 1979 ECS—The Electrochemical Society.

the electrode kinetics.[130−132] Another key issue is the resistivity of the contact between the active oxide and the support, which has been shown to be particularly high in the case of certain TiO_2−MO_x anodes.[113] In cases where high conductivity is expected, a highly porous electrode exhibits greatly enhanced activity per geometric area relative to a smooth surface. One approach to preparing high surface area oxides is the in situ generation of the oxide layer by anodization of a high surface area metallic substrate. Ni oxides have shown modest activity for the OER in alkaline media, and accordingly anodization of a Raney Ni substrate produces a highly active NiO_x anode.[133] While preparation of a porous metal precatalyst is one route to produce a porous active anode, an alternative route involves electrodeposition of a highly porous hydrous oxide from solution-based precursors.[134,135] Most often, these hydrous oxides exhibit much higher activity per geometric area relative to those sintered at high temperature but exhibit poorer stability and corrosion resistance. A potential compromise between activity and stability may be achieved by fashioning oxide nanoparticles as active anodes. This has been demonstrated in the case of IrO_2[136] and Co_3O_4,[137] but further work to extend this methodology to a wider array of transition metal oxides is needed.

Most first-row transition metal oxides are susceptible to corrosion under acidic conditions. The protons produced from water splitting can dramatically lower the pH in the vicinity of the electrode. At some critical pH, the hydronium ion concentration will be sufficient to protonate the oxide itself, resulting in corrosion. For this reason, the stability of metal oxide anodes is enhanced when operated under harsh alkaline conditions. However, operation under these conditions incurs significant balance-of-systems costs[138] and hence water-splitting technologies remain expensive for nonconcentrated solar energy storage applications.[139] The corrosion issue has been overcome by the discovery of a self-healing catalyst.[140] Highly active cobalt-based[141] and nickel-based[142] oxygen evolving catalysts self-assemble from aqueous solutions as a thin film on conductive[143] or semiconductive[104−106] substrates. The catalysts are molecular in nature even though they operate as a heterogeneous system. Because of the self-healing process, the cobalt phosphate (Co−Pi) catalyst operates in simple buffered aqueous solutions over a wide pH range (>4.5) and in natural waters. They are indeed functional models of the oxygen-evolving complex of Photosystem II.[144] The simple operation of the catalysts from conventional water sources under benign conditions is an important step toward providing distributed solar energy storage at low cost.[145]

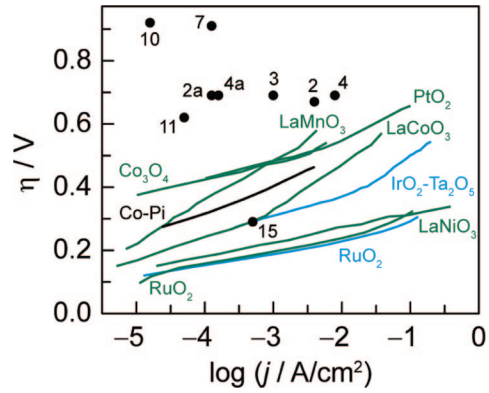

Figure 9. Selected activity data for extended solid-state and molecular OER catalysts. Plots and data points are extracted from figures or data presented in the stated references. Polarization data for extended solids collected under alkaline (green solid lines) and acidic (cyan solid lines) conditions are shown along with single point data for molecular compounds (black circles). Polarization data are also shown for the cobalt phosphate (Co−Pi) catalyst that operates in water at pH 7 (black solid line) (ref 141). Conditions for molecular catalysts are **2**: $[Ru^{III}(NH_3)_5Cl]^{2+}$ on Pt black, 0.1 M $NaClO_4$, pH 6.8 (ref 169); **2a**: $[Ru^{III}(NH_3)_5Cl]^{2+}$ on Nafion, 0.1 M KNO_3, pH 5.4 (ref 168); RuO (cyan solic lines) on Ti, 1 M H_2SO_4 (ref 146); **3**: $[(NH_3)_5Ru^{III}(\mu\text{-}O)Ru^{III}(NH_3)_5]^{4+}$ in Nafion, 0.1 M KNO_3, pH 5.4 (ref 171); **4**: $[(NH_3)_5Ru(\mu\text{-}O)Ru(NH_3)_4(\mu\text{-}O)Ru(NH_3)_5]^{6+}$ on Pt black, 0.1 M $NaClO_4$, pH 6.8 (ref 175); **4a**: $[(NH_3)_5Ru(\mu\text{-}O)Ru(NH_3)_4(\mu\text{-}O)Ru(NH_3)_5]^{6+}$ on Nafion, 0.1 M KNO_3, pH 5.4 (ref 172); **10**: $[Ru(Mebimpy)(4,4'\text{-}((HO)_2\text{-}OPCH_2)_2bpy)(OH_2)]^{2+}$ adsorbed on ITO, 0.1 M HOAc/NaOAC, pH 5 (ref 184); **11**: $[Mn_4O_4((p\text{-}MeOPh)PO_2)_6]^{+}$ in Nafion, 0.1 M Na_2SO_4, pH 11 (ref 185); **15**: colloidal IrO_2 nanoparticles, 0.1 M NaOH, pH 13 (ref 193); RuO_2 (green solid lines) on Ti, 1 M NaOH (ref 146); $LaNiO_3$ pressed pellet, 1 M NaOH (ref 119); IrO_2−Ta_2O_5 on Ti in 0.5 M H_2SO_4 (ref 147); $LaCoO_3$ pressed pellet, 1 M NaOH (ref 119); $LaMnO_3$ pressed pellet, 1 M NaOH (ref 119); Co_3O_4 on Ti in 1 M KOH (ref 148); PtO_2 bonded in fluorinated ethylene propylene in 5 M KOH (ref 122).

Figure 9 benchmarks the activity of extended solid-state and molecular OER catalysts based on steady-state polarization data. These data comprise a small fraction of the wide array of electrodes evaluated for OER activity and are meant to be representative of the best in class for various types of materials, strategies, and operating conditions. Because temperature has an appreciable impact on electrode activity, the activities of various catalyst systems are compared at ambient temperature (ca. 25 °C). The data presented are meant only as an *estimate* of the relative performance of different materials because disparities in the *effective surface area* of the anode is *unknown*. A rigorous comparison of catalyst performance requires the knowledge of accurate surface areas and controlled conditions. Nevertheless, the data in Figure 9 offer the strictest comparison of catalytic activity because data are reported for catalysts that provide activity as a function of overpotential under electrocatalytic conditions (vs chemical conditions).

Several general trends become evident from the compilation of data summarized in Figure 9. Ir and Ru oxides exhibit excellent activities for the OER in both acidic and alkaline conditions. First-row transition metal oxides exhibit moderate to excellent activity with $LaNiO_3$ showing the best performance in alkaline media. PtO_2 exhibits poor activity for the OER along with oxides of mid to early transition metals (e.g., Mn). The data also highlight the paucity of nonprecious metal catalysts that operate under acidic conditions; this explains the current

emphasis on the discovery of earth-abundant catalysts that are both stable and active at moderate to low pH.

5.3.2. Molecular OER Catalysts

Investigation of molecular OER catalysts has been studied in large part because of their relevance to photosynthesis.[12,149,150] Several molecular inorganic constructs have been developed that can catalyze the production of O_2 from water. In many of these systems, a sacrificial oxidant such as Ce^{IV} (which has a standard reduction potential of 1.72 V[151]) is used (in place of an electrode or photoelectrode) to regenerate the catalyst. However, for solar energy storage, an electrocatalyst (indirect) or photoelectrocatalyst (direct) is preferred. Additionally, technology applications of these catalysts require that they be active *and* stable for long-term operation. While many reports detail the activity of the molecular water oxidation catalysts, there is often little data describing the long-term stability of these materials.

Molecular OER catalysts have been treated extensively in the review literature including surveys of Mn_4O_4 cubanes[152] and ruthenium diimine complexes,[153,154] in addition to general reviews on the topic of oxygen evolution by molecular species.[155,156] A complete review of molecular OER catalysts is hence not warranted here. Rather, this section focuses on molecular OER electrocatalysts of Chart 1 so that a side-by-side comparison may be made to extended solid-state electrocatalysts of section 5.3.1.

5.3.2.1. Ruthenium Polypyridine and Ammine Catalysts. The landmark molecular OER catalyst is the blue dimer, $[(bpy)_2(H_2O)Ru^{III}(\mu\text{-}O)Ru^{III}(OH_2)(bpy)_2]^{4+}$ (**1**) (bpy = 2,2′-bipyridine), first reported in 1982.[157] Initial reports of an apparent catalytic wave 0.1 M H_2SO_4 was later attributed to chloride oxidation.[158] More detailed studies of the blue dimer in CF_3COOH established OER with a measured current efficiency of 19% and limited turnover number.[159] Elucidating the mechanism of catalysis by the blue dimer is an ongoing pursuit.[160−167]

The blue dimer has been a springboard for the development of mono-, di-, and trinuclear ammine-ligated ruthenium OER catalysts. Frequently, these ruthenium ammine complexes are embedded in membranes or solid materials and turnover is driven by a chemical oxidant. However, electrochemical data are available for some ammine−ruthenium complexes. The mononuclear complex $[Ru^{III}(NH_3)_5Cl]^{2+}$ (**2**) has been immobilized in a Nafion membrane and interrogated electrochemically.[168] Current density and turnover frequency are dependent on catalyst loading. The TON maximizes at 4.7 for the first hour of catalysis when the catalyst concentration is 0.1 M; the maximum current density of 0.12 mA/cm^2 is achieved with an applied overpotential of 0.69 V for a catalyst at a concentration of 0.7 M in the Nafion membrane. The same complex, when adsorbed onto Pt black, performs better, and current densities of 3.8 mA/cm^2 are observed for bulk electrolysis carried out at 0.67 V overpotential and pH 6.8.[169] The dinuclear $[(NH_3)_5Ru^{III}(\mu\text{-}O)Ru^{III}(NH_3)_5]^{4+}$ (**3**) is a structural analogue of the blue dimer,[170] and the compound promotes the OER reaction when embedded in a Nafion membrane.[171] Steady-state bulk electrolysis data are not available, but from cyclic voltammetry traces, a current density of 1.1 mA/cm^2 is estimated at an overpotential of 0.69 V at pH 5.4 in KNO_3 electrolyte; the catalyst is unstable, and a TON of 2.7 is observed for the first hour of electrolysis. More extensive studies have been performed on the trinuclear complex $[(NH_3)_5Ru(\mu\text{-}O)Ru(NH_3)_4(\mu\text{-}O)Ru(NH_3)_5]^{6+}$ (**4**) on different electrode supports. Incorporated into a Nafion membrane, **4** exhibits a maximum TOF of 10.7 h^{-1} (for 1 h of catalysis).[172] The steady-state current increases with catalyst concentration; at a concentration of ca. 0.22 M and an applied overpotential of 0.69 V, **4** was observed to drive OER at an average current of 0.17 mA/cm^2. The catalytic activity of the Nafion/Ru-red composite was shown to increase in the presence of amino acid mimics.[173,174] For example, a ∼5-fold enhancement in the TOF was observed when *p*-cresol was used as the mediator. Catalyst activity is observed to increase with the deposition of **4** on Pt black, presumably due to a higher catalyst loading. The observed current density of ∼8 mA/cm^2 at an overpotential of 0.67 V at pH 6.8 is 8.3 times higher than that observed for Pt black without the catalyst.[175] On a gold electrode, the performance of the catalyst is considerably worse (η = 0.77 V, average current density of only 1.0 mA/cm^2, ∼2.9 times greater than the unmodified gold electrode).[176]

Several other ruthenium complexes have been reported to catalyze water oxidation, either chemically or electrochemically. A $Ru^{III}(\mu\text{-}O)Ru^{III}$ core, similar to the blue dimer but featuring a second bridging bipyridyl ligand, was shown to oxidize water electrocatalytically. Although many details of the steady-state electrolyses are omitted, a turnover number of 4.7 h^{-1}, with a current efficiency of 90%, was reported.[177] Another $Ru^{III}(\mu\text{-}O)Ru^{III}$-containing molecule, $[(tpy\text{-}PO_3H_2)(H_2O)_2RuIII]2O4+$ (**5**), adsorbed onto an ITO electrode attains a TON maximum of 3.0 with an applied overpotential of 0.58 V at pH 6.[178] Even higher TONs are observed for an electropolymerized diruthenium complex possessing pendant pyrrole groups, $[Ru_2(\mu\text{-}bpp)(\mu\text{-}OAc)(t\text{-}trpy)_2]^{2+}$ (**6**) ((bpp = bis(2-pyridyl)pyrazolato, t-trpy = 4′-(*para*-pyrrolylmethylphenyl)-2,2′:6′,2″-terpyridine);[179] with an applied overpotential of 0.24 V, a TON of 120 was obtained for one of the electrode compositions.

Tanaka and co-workers have found that the dinuclear quinone-chelated, anthracene-bridged ruthenium complex $[Ru_2(OH)(3,6\text{-}^tBu_2qui)_2(btpyan)](SbF_6)_2$ (**7**) (qui = quinone, btpyan = 1,8-bis(2,2′:6′,2″-terpyridyl)anthracene) catalyzes water oxidation from an indium tin oxide (ITO) surface.[180,181] With an applied overpotential of 0.91 V, a current density of 0.12 mA/cm^2 was reported. Although the compound eventually does decompose, the species possesses some of the highest OER production rates for a molecular catalyst, attaining an average turnover frequency of ca. 840 h^{-1} over a 40 h period.

Many of the foregoing ruthenium complexes possess at least two metal centers, which are proposed to work in concert during OER. Very recently, mononuclear $[Ru^{III}(tpy)(bpm)(OH_2)]^{2+}$ (**8**) and $[Ru^{III}(tpy)(bpz)(OH_2)]^{2+}$ (**9**) (tpy = 2,2′:6,2″-terpyridine, bpm = 2,2′-bipyrimidine, bpz = 2,2′-bipyrazine) complexes have been reported to effect OER using Ce^{IV} to drive the reaction.[182] Monoruthenium tpy-bound complexes possessing several different bidentate ligands are also competent OER catalysts under acidic conditions.[183] Surface confinement of the catalyst to an electrode has been achieved via the phosphonate linkers of $[Ru(Mebimpy)(4,4'\text{-}((HO)_2\text{-}OPCH_2)_2bpy)(OH_2)]^{2+}$ (**10**) (Mebimpy = 2,6-bis(1-methylbenzimidazol-2-yl)-pyridine).[184] With a surface coverage of 1.2×10^{-10} mol/cm^2 on fluorine-doped SnO_2 (FTO), **10** has been shown to support a current density of 14.8 μA/cm^2 at an applied overpotential of 0.92 V at pH 5. This current density corresponds to a turnover frequency of 0.36

Chart 1

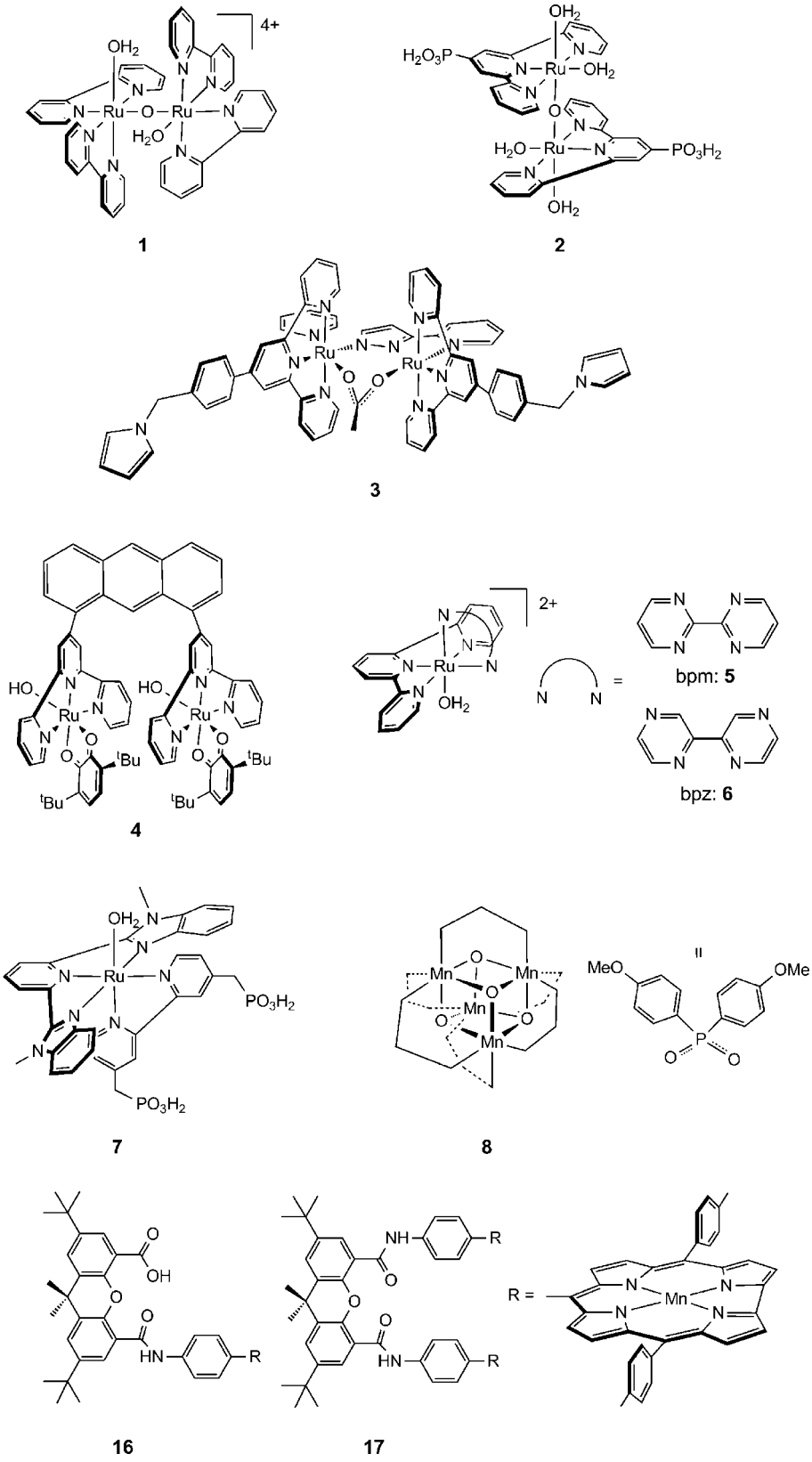

s^{-1} for an 8 h electrolysis. An electrode prepared in this manner is less active at pH 1, exhibiting a current density of 4.9 μA/cm^2 with an applied overpotential of 0.68 V, which corresponds to a TOF of 0.12 s^{-1}.

5.3.2.2. Inorganic Clusters. Motivated in large part by the structure of the OEC in Photosystem II, tetramanganese clusters have been interrogated as catalysts for water oxidation. As a Nafion composite, a Mn_4O_4 complex bridged by bis(4-methoxyphenyl)phosphinate ligands, $[Mn_4O_4((p\text{-MeOPh})PO_2)_6]^+$ (**11**) is proposed to drive OER under white light illumination and an applied potential.[185] The photocurrent scales linearly with pH when the applied potential is held at a constant 1.2 V vs NHE. When the electrode is illuminated with >275 nm white light (150 mW/cm^2) at pH 11, an initial

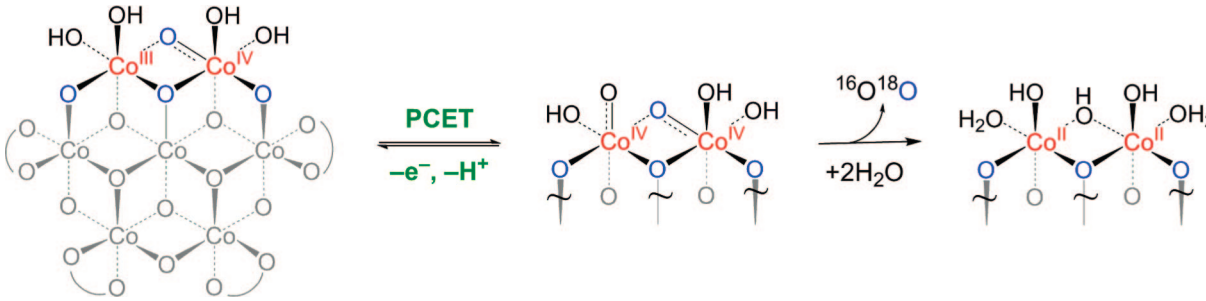

Figure 10. Proposed pathway for OER by Co−Pi. A PCET equilibrium proceeded by a turnover-limiting O−O bond forming step is consistent with current dependencies on proton and electron equivalencies. Curved lines denote linkages to either phosphate, water, and/or hydroxide terminal ligands.

photocurrent density of 9 μA/cm^2 is reported. This current is not stable, showing an average decrease of ca. 0.7 μA/cm^2 per h over the course of 10 h. The need for white light and applied potential amounts to this catalyst operating at a very large overpotential.

All-inorganic clusters have the advantage that they can be intrinsically more stable because organic ligands are absent. This is certainly the case for the heterogeneous molecular cobaltate cluster of Co−Pi, which exhibit superior stability owing to the self-repair mechanism and presence of only oxygen and inorganic phosphate or borate ligands. Polyoxometallates are also capable ligands of OER centers. A mixed polyoxometallate cluster containing a diruthenium core, $[Ru^{III}_2Zn_2(H_2O)_2(ZnWO_{34})_2]^{14-}$ (**12**), drives OER though steady-state current densities are unknown as the OER reaction was investigated by pulsed voltammetry.[186] A Tafel slope of 120 mV is quoted, indicating that the turnover-limiting step is associated with electron transfer. A Ru_4 polyoxometallate, $[Ru_4(H_2O)_4(\mu\text{-}O)_4(\mu\text{-}OH)_2(\gamma\text{-}SiW_{10}O_{36})_2]^{10-}$ (**13**) also catalyzes OER; electrochemical data are scant, a TON of 7.5 is reported when the complex is electrolyzed at 0.2 V overpotential, pH 0.6.[187] This same cluster can catalyze OER using $Ru(bpy)_3^{3+}$ as a stoichiometric oxidant.[188,189]

Very recently, a cobalt-containing polyoxometallate cluster, $[Co_4(H_2O)_2(PW_9O_{34})_2]^{10-}$ (**14**), was reported as an active water oxidation catalyst.[190] The catalyst was primarily studied using $[Ru(bpy)_3]^{3+}$ as a sacrificial oxidant, though the electrochemical performance can be estimated from a cyclic voltammogram. Measured at pH 8, the catalytic onset is observed at ca. 200 mV overpotential, although in the absence of a reported electrode area the current density cannot be estimated from this same plot.

5.3.2.3. Iridium Complexes. Cyclometalated bis-phenylpyridine diaquo iridium(III) complexes, which could be tuned by varying the substitution on the phenylpyridine ligand, were studied as water oxidation catalysts.[191] Additionally, iridium(III) complexes ligated by pentamethylcyclopentadienyl (Cp*) are reported to be even more active for water oxidation.[192] However, both of these reports lacked detailed electrochemical characterization and therefore are not included in Figure 9 or discussed further.

Solution nanoparticles of IrO_2 (**15**) are at the boundary between molecular and solid-state catalysts. At pH 13 in a rotating ring disk electrode experiment, IrO_2 oxidizes water at a Faradaic efficiency of 100% and a current density of 0.5 mA/cm^2 at 0.29 V overpotential.[193]

5.3.2.4. Macrocyclic OER Catalysts. Porphyrins and corroles presented in Pacman and Hangman motifs[194,195] have been reported as OER catalysts. Two porphyrins juxtaposed via an *o*-phenylene spacer furnish a Pacman complex that promotes OER from acetonitrile/water mixtures[196] at a catalytic onset potential of 1.4 V vs NHE. Electrochemical characterization of the system is minimal, making it difficult to judge the OER performance of these catalysts, although a Faradaic efficiency of only 5−17% is reported; the highest activity results when the porphyrin meso positions contain pentafluorophenyl substituents. Hangman manganese corrole **16** and Pacman manganese corrole **17** have also been shown to split water electrochemically.[197] Catalytic activities of the compounds for electrochemical water oxidation were studied by CV. The oxidation potentials were reported at $E_{pa} = 0.79$ V, and $E_{pa} = 0.80$ V [*n*-BuNOH (10% in water) in CH_2Cl_2/CH_3CN (2/3) v/v], for **16** and **17**, respectively. The oxygen evolution was also investigated with an oxygen-sensing electrode. The solution containing **16** (5 μmol) was electrolyzed at 0.85 V. Over the course of a 13 min of electrolysis, the concentration of O_2 in deionized water increased from 3.00 to 19.2 μM in the initial 1.5 min. The same experiment was performed with **17**. The concentration of O_2 increased from 1.5 to 47.50 μM within the initial 1.5 min. This study shows that compound **17** (the Pacman system) has higher catalytic efficiency for water oxidation than **16** (the Hangman system) under basic conditions.

A nitro-modified Mn(III) corrole has also been reported to split water when treated splitting with *t*-BuOOH.[198] The formation of Mn(V) was observed in situ by UV−vis spectroscopy and high-resolution mass spectrometry (HRMS). The amount of generated oxygen was determined with mass spectrometry analysis; however, this system was not characterized electrochemically, and thus a comparison to other OER catalysts described herein is not possible.

5.4. Comparison of Extended Solid-State and Molecular OER Catalysts

As shown in Figure 9, when electrodes are prepared with molecular catalysts and compared to extended solids, with the exception of Co−Pi and as much as IrO_2 nanoparticles **15** are molecular, they are not as active. Nevertheless the molecular catalysts do offer the advantage that detailed mechanistic studies of OER may be undertaken. In this regard, the Co−Pi catalyst is unique inasmuch as it provides a molecular bridge to extended solids, and in doing so provides mechanistic insight into solid-state OER. Tafel data and isotope labeling studies[297] and XAS[298] and EPR[299] spectra of active catalysts films all point to the mechanism shown in Figure 10 for the molecular cobaltate cluster (MCC) model derived from XAS studies. The rate law is consistent with a PCET pre-equilibrium preceding the turnover-limiting O−O

bond forming step from a Co^{IV} formal oxidation state. Isotopic labeling experiments suggest the source of the oxygens to be from a terminal oxo that couples to a bridging oxo/hydroxo. The OER activity of MCC unit of Co−Pi is in striking contrast to the properties of solid-state cobaltate materials. Sodium cobaltates with Co valencies ≥3.4 are stable to water across the pH spectrum.[199−202] This stability is not the result of limited contact between H_2O and the Co ions; H_2O and H_3O^+ molecules readily intercalate between the CoO_2 planes. Evidently, the extended CoO_2 planes in the cobaltates support high Co valencies while remaining resistant to water oxidation. In contrast, the high catalytic activity of Co−Pi suggests that the MCCs promote water oxidation if the Co valency is greater than 3. One often hears the phenomenological contention that edges are important in solid-state catalysis. The contrast of the MCC to extended cobaltates bears this out. The OER mechanism in Figure 10 requires a terminal water, which is achieved at the "edge" of the MCC. By truncating the extended cobaltate lattice at a molecular dimension, the number of edges is maximized and maximum activity is realized. The extended cobaltate lattices have few terminal oxygens and hence are unable to support OER.

Finally, it should be noted that the majority of OER catalysts listed in section 5.3.2 are based on metals (Mn, Ir, Ru) whose oxides are active OER catalysts (MnO_2, IrO_2, RuO_2). Most of the molecular catalysts have TONs that could be supported by extremely small quantities of the oxide as a contaminant. It is therefore paramount to establish that OER activity is due to the molecule and not to oxide nanoparticles formed from the decomposition of the molecular complex.

5.5. Catalysts for the Hydrogen Evolution Reaction (HER)

5.5.1. Extended Solid-State HER Catalysts

The hydrogen evolution reaction (HER) has been studied extensively for nearly every transition metal.[203,204] The generally accepted HER mechanism at metal electrodes in acidic media consists of a sequence of the three steps shown below.[205] The first of these is the Volmer or discharge step:

$$H^+_{(aq)} + e^- \rightarrow H_{ads} \quad (22)$$

A surface adsorbed hydrogen atom (H_{ads}) is generated by coupling a single electron transfer at the interface with proton transfer to the surface. After generation of H_{ads}, the reaction can proceed by recombination of two surface adsorbed H atoms to generate H_2 upon desorption (Tafel step):

$$2H_{ads} \rightarrow H_2 \quad (23)$$

and/or by protonation of H_{ads} coupled to a single electron transfer (Heyrovsky step):

$$H_{ads} + H^+_{(aq)} + e^- \rightarrow H_2 \quad (24)$$

As might be expected, the strength of the H_{ads}−metal interaction plays a critical role in determining the catalytic activity of the metal electrode. Indeed, a plot of the log of the exchange current densities (j_0) for the HER in acidic media vs the energy of chemisorption of hydrogen for a wide array of metals yields the volcano-shaped linear free energy relationship shown in Figure 11.[206] Gerischer[207] and Parsons[208] originally rationalized this relationship by deducing that the enthalpy of chemisorption, H_{ads}, is proportional to the ΔG of hydrogen adsorption ($\Delta G - H_{ads}$) at the thermodynamic potential for proton reduction. The right-hand branch of the experimental volcano plot corresponds to metals for which $\Delta G - H_{ads}$ is large and negative. In this situation, the adsorbate forms a strong bond with the surface, making the initial discharge step facile but significantly retarding the subsequent protonation or recombination steps. The left-hand branch corresponds to metals for which $\Delta G - H_{ads}$ is large and positive. In this case, H_{ads} interacts weakly with the surface, leading to a slow discharge step that limits the turnover rate. The volcano curve peaks in the vicinity of Pt for which $\Delta G - H_{ads}$ is believed to be near zero. The forgoing explanation, therefore, is an application of the Sabatier principle[209] to hydrogen evolution electrocatalysis. $\Delta G - H_{ads}$ is difficult to measure experimentally, but recent computational efforts have provided support for the interpretation of Gerischer and Parsons by calculating the $\Delta G - H_{ads}$ for a number of metal surfaces.[210] A plot of the log of experimental j_0 values versus the computed values for $\Delta G - H_{ads}$ yields a volcano curve centered at a $\Delta G - H_{ads} = 0$.

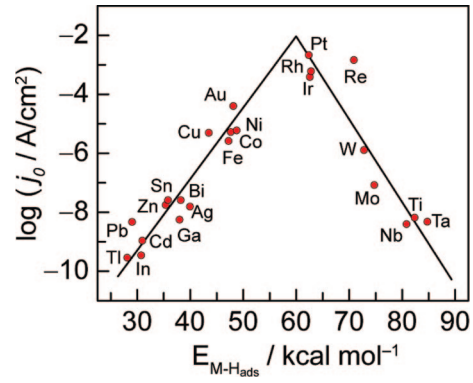

Figure 11. Volcano curve for the HER on metal electrodes in acidic media. The log of the exchange current density j_0 is plotted versus the M−H bond energy for each metal surface. Reprinted with permission from ref 206. Copyright 1972 Elsevier.

Although the above comparisons of j_0 provide valuable insight into periodic trends, they serve only to characterize the HER at equilibrium conditions, $\eta = 0$. In any practical device, the cathode may be poised at hundreds of millivolts overpotential and therefore the Tafel slope for a given material plays a prominent role in determining its utility.[211] Furthermore, the paucity of reliable polarization data has prevented a thorough analysis of HER in alkaline media.[212] The HER mechanism may change drastically for a particular metal between the two pH extremes.[213−215] Future efforts to better characterize linear free energy relationships for the HER in alkaline media will be valuable in the context of alkaline electrolysis.

One technological hurdle evident from Figure 11 is that precious metals are found to possess the greatest HER activity under equilibrium conditions for a monometallic catalyst. In an effort to move away from precious metals, numerous studies have focused on developing bi- or multimetallic alloys or intermetallic materials in an effort to tune $\Delta G - H_{ads}$ and, thereby, increase electrocatalytic activity.[216,217] Binary alloys or intermetallics consisting of a metal from the left- and right-hand branches of the volcano plot have exhibited significantly improved activity relative to either metal by itself. A well-controlled study alloyed Ni, a metal

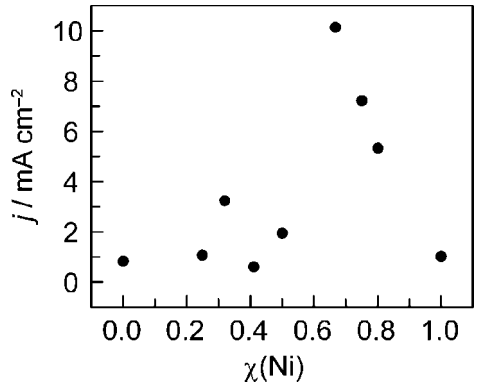

Figure 12. Steady-state HER current density at 300 mV overpotential as a function of the mole fraction of Ni in Ni−Ti binary alloy. Reprinted with permission from ref 217. Copyright 1997 Elsevier.

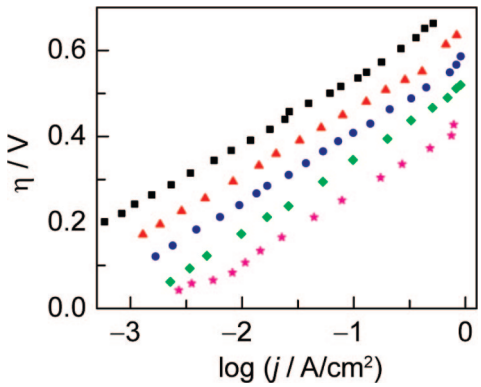

Figure 13. Quasi-steady-state Tafel plots of the HER on unactivated Ni (black solid square) and Ni subjected to cathodic activation in 0.5 M H_2SO_4 in presence of 1 (red triangles), 2 (blue circles), 4 (magenta stars), and 8 (green diamonds) g/L of $H_3PMo_{12}O_{40}$. Reproduced with permission from ref 225. Copyright by 1992 ECS—The Electrochemical Society.

which adsorbs hydrogen weakly, with Ti, a metal which adsorbs hydrogen very strongly.[218] A plot of the steady-state current density for the HER on smooth Ni−Ti alloy electrodes at $\eta = 300$ mV vs the Ni content shows that the Ni_3Ti intermetallic phase exhibits 1 order of magnitude improved activity relative to either pure metal (Figure 12). Similar synergistic effects have been observed for an array of alloys (e.g., Mo−Ni,[109,219,220] Mo−Co,[221] Mo−Pt,[222] Ni−Zr,[216] Mo−S[223]). However, in some of these cases, it is difficult to ascertain whether the improved activity arises from increases in surface roughness or intrinsic improvement in catalyst activity.

Heteropolyacids (HPAs) serve as activators of a given metal during or following metal deposition. These HPAs are believed to bind strongly and irreversibly to the metal surface under conditions of electrocatalytic turnover.[217] The ionic interaction of the HPA with the metal surface is proposed to induce a change in the d-band position of the metal and thereby modulate $\Delta G - H_{ads}$. In some cases, the HPA itself may serve as the electrocatalyst.[224] One example of HPA mediated electrode activation is shown in Figure 13.[225] In this study, a bare nickel electrode was electrolyzed at a constant cathodic current density (0.5 A/cm^2) in the presence of varying concentrations of $H_3PMo_{12}O_{40}$ in 0.5 M H_2SO_4 until the electrode potential stabilized. The electrode was transferred to 3 M KOH, and current−voltage characteristic were evaluated in the absence of any HPA in solution. The polarization data of Figure 13 show maximum activity for a 4 g/L of $H_3PMo_{12}O_{40}$. This simple activation procedure leads to activity improvements of approximately 2 orders of magnitude over a wide range of overpotentials. Similar activation procedures using HPAs have been employed to improve the activity of other metals (e.g., Co,[226] Pd,[227] Fe[228]), although several ambiguities remain unresolved. It is unclear to what extent surface roughness is enhanced in the activation procedure. Additionally, XPS studies of the modified surface suggest that the HPA is subject to partial decomposition[225] during the activation process, making it difficult to establish the precise mechanistic role played by the activator. Nonetheless, the simplicity of solution-based methods for electrode activation suggests a renewed research effort in this area may be fruitful.

One key advantage of utilizing metal electrodes as catalysts is the ease with which the surface roughness can be greatly enhanced while maintaining electrical conductivity throughout the porous substrate. Dealloying is an especially effective surface roughening method. This procedure affords electrodes with roughness factors on the order of 50 000, leading to dramatic activity improvements. For example, Raney Ni[229] is prepared by electrochemically or chemically leaching aluminum from Ni−Al alloys.[230] Raney Ni cathodes exhibit activity profiles rivaling those of planar platinum.[231] Dealloyed binary alloys may also be prepared from ternary starting materials to increase surface area while retaining the synergistic benefits to HER activity that are provided by intermetallic phases.[232]

Benchmark steady-state polarization data for a selected array of cathode materials are presented in Figure 14. These data comprise a small fraction of the wide array of electrodes evaluated for HER activity[203] and are meant to be representative of the best in class for various types of materials, strategies, and operating conditions. As for Figure 9, a rigorous comparison of catalyst performance requires the knowledge of accurate surface areas and controlled conditions. From this compilation, several general trends become evident. Proton reduction under alkaline conditions can proceed at useful current densities (~100 mA/cm^2) using high surface area cathodes consisting entirely of earth abundant first-row transition metals or metal alloys. The success of HER catalysis under alkaline conditions, however, is not realized in acidic media. Precious metals and precious metal oxides have remained the materials of choice for proton reduction in acid. First-row transition metals in acidic media exhibit activities several orders of magnitude lower than their precious metal counterparts. The strategies described above for improving performance of HER catalysts in alkaline media do not translate to improved performance under acidic conditions. As such, many recent efforts have focused on developing molecular catalysts consisting of first-row transition metal ions that may be able to fill the activity gap observed for metal electrodes.

5.5.2. Molecular HER Catalysts

Studies of molecular HER catalysts are motivated invariably by the need to replace precious metal cathodes, namely platinum, with more earth-abundant materials. The long-term goal of this research effort is to develop catalysts that operate in aqueous environments, however, many molecular electrocatalysts reported to date are only stable/active in organic solvents or organic/aqueous solvent mixtures. The operation of catalysts in nonaqueous solvents makes it difficult to make comparative assessments of molecular HER catalysts owing

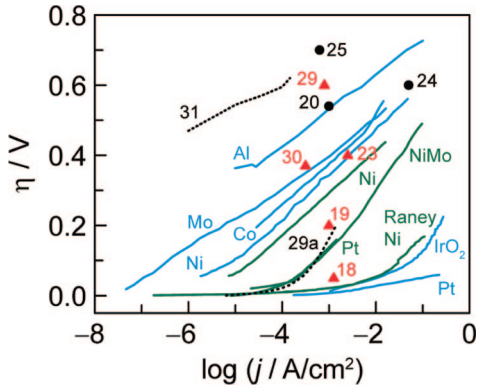

Figure 14. Selected activity data for HER catalysts. Plots and data points are extracted from figures or data presented in the stated references. Polarization data for extended solids collected under alkaline (green solid lines) and acidic (cyan solid lines) conditions are shown along with data for molecular compounds evaluated in acetonitrile (red triangles) and in water (black circles and square-dotted lines). Polarization data are also shown for a molecular catalyst immobilized on MWCNT (—) and evaluated under acidic conditions. Conditions for each catalyst: **18**: $Co^{III}(dmgH)_2(Py)(Cl)$ in CH_3CN containing 0.2 M $Et_3NH(BF_4)$ (ref 245); **19**: $Co(dmgBF_2)(CH_3CN)_2$ in CH_3CN containing 0.045 M CF_3COOH (ref 246); **20**: Co-tetraimine adsorbed onto glassy carbon in water at pH 2 (ref 250); **23**: $Co(PY4)(CH_3CN)_2$ in CH_3CN containing 0.026 M CF_3COOH (ref 252); **24**: Co and Pt porphyrins adsorbed onto glassy carbon in 1 M $HClO_4$ (ref 255); **25**: Co-phthalocyanin electropolymerized onto glassy carbon in phosphate buffer, pH 2.4 (ref 256); **29**: $[Ni(P_2^{Ph}N_2^{Ph})_2(CH_3CN)](BF_4)_2$ in CH_3CN containing 0.034 M CF_3SO_3H (ref 272); **29a**: a derivative of **29** attached to MWCNT in 0.5 M H_2SO_4 (ref 274); **30**: $CpMo(\mu\text{-}S)_2S_2CH_2$ in CH_3CN containing 0.031 M *p*-cyanoanilinium (ref 275); **31**: $[(PY5Me_2)MoO](PF_6)_2$ in 0.6 M phosphate buffer at pH 7 (ref 276); smooth Pt (cyan solid lines) in 1 M H_2SO_4 (ref 233); IrO_2 in 1 M H_2SO_4 (ref 234); activated Pt (green solid lines) in 0.1 M NaOH (ref 235); Raney Ni in 1 M KOH (ref 231); NiMo in 1 M NaOH (ref 211); smooth Ni (green solid lines) in 1 M NaOH (ref 211); smooth Ni (cyan solid lines) in 1 M $HClO_4$ (ref 236); smooth Co in 0.5 M H_2SO_4 (ref 237); smooth Mo in 0.1 M HCl (ref 238); smooth Al in 0.25 M H_2SO_4 (ref 239).

to varying proton activity, although recent reports do detail the proper treatment of the thermodynamics of nonaqueous proton reduction.[240]

Chart 2 collects the chemical structures of the molecular HER catalysts discussed below. Electrochemical parameters used in the comparison of these HER catalysts are primarily furnished from the interpretation of cyclic voltammetry traces available in the referenced works. As described by Evans,[240] values of overpotential and current density are estimated from the point where the catalytic current reaches half of its maximum value.

5.5.2.1. Nickel and Cobalt Macrocycles. First-row transition metal ions ligated by nitrogen-donor macrocycles comprise a pre-eminent class of HER catalysts. Dual CO_2 and proton reductions were reported for a series of Ni^{II} and Co^{II} tetraazamacrocycles[241] over 30 years ago, with subsequent reports demonstrating electrocatalytic proton reduction by Ni^{II}-cyclam with overpotentials in excess of 1 V and current densities of less than 10 $\mu A/cm^2$.[242] More recently, Co^{II} complexes of hexadentate azamacrocycles demonstrate H_2 evolution over a range of pH values; the overpotential at pH 2.0 is ~0.8 V.[243]

Cobalt diglyoxime complexes, which were shown over 20 years ago to catalyze proton reduction in the presence of chemical reductants in aqueous HCl,[244] have been the subject of much electrochemical scrutiny of late. Simultaneous reports established the electrocatalytic hydrogen evolution by $Co^{III}(dmgH)_2(Py)(Cl)$[245] (**18**) and related Co^{II} complexes of difluoroboryl-glyoxime macrocycles,[246] which have been subsequently elaborated to other tetra-imine ligand platforms.[247,248] The majority of work has been performed in nonaqueous solvents with a variety of different acids. Bulk electrolysis of **18** in acetonitrile with 0.2 M $Et_3NH(BF_4)$ gives an average current density of 1.2 mA/cm^2 and an average turnover frequency of 4.7 ± 2 h^{-1} with an applied overpotenial of ca. 50 mV.[249] Complexes with difluoroboryl bridges are reported to catalyze proton reduction at overpotentials as low as 40 mV. When bulk electrolysis of $Co(dmgBF_2)(CH_3CN)_2$ (**19**) in acetonitrile is conducted at 0.2 V overpotential in the presence of 45 mM CF_3COOH, turnover frequencies as high as 20 h^{-1} have been reported.[246] Current density values are not quoted for bulk electrolysis experiments but can be estimated to be ~1 mA/cm^2 from cyclic voltammetry under similar conditions. All of the aforementioned electrocatalytic studies were carried out in nonaqueous environments, although a recent report of Co-tetra-imine complexes (**20**) adsorbed onto glassy carbon electrodes includes electrocatalytic measurements in acidic aqueous solution.[250] At pH 2, onset of catalysis occurred at 0.24 V overpotential, and bulk electrolysis at 0.54 V overpotential operated at ~1 mA/cm^2 with 80 ± 10% Faradaic efficiency.

Several other coordination complexes have been studied as electrocatalysts for proton reduction. Cobalt clathrochelates, which are boron capped tris(glyoximato) complexes similar to the bis(glyoximato) class of complexes discussed above, have been found to exhibit electrocatalytic proton reduction.[251]

Chart 2 depicts the structures of two cobalt clathrochelates whose electrocatalytic properties are considered. With these complexes, the overpotential for H_2 evolution is 0.4 V when R = Ph (**21**) and 0.8 V when R = Me (**22**).

A cobalt ion coordinated by tetradentate 2-bis(2-pyridyl)-(methoxy)methyl-6-pyridylpyridine (PY4), $Co(PY4)(CH_3CN)_2$ (**23**) reduces protons in acetonitrile solution mixtures containing up to 50% water.[252] In acetonitrile solution, where calculation of overpotential is straightforward, the catalyst reduces trifluoroacetic acid with an overpotential of 400 mV, and when 1.0 mM of **22** is in the presence of 26.0 mM of the acid, a current density of ca. 2.7 mA/cm^2 is observed by cyclic voltammetry. Controlled-potential electrolysis experiments establish a Faradaic efficiency of 99%.

Metalloporphyrins have also been studied for proton reduction electrocatalysis. Cobalt porphyrins operate with overpotentials of 0.6 V in solution[253] and <0.2 V at pH 7 when covalently attached to glassy carbon.[254] Mixed Co(II)/Pt(II) porphyrin systems (**24**), coated onto glassy carbon, catalyze proton reduction with 0.6 V overpotential, with reported current densities of >50 mA/cm^2.[255] A recent paper details electrochemical studies of thiophene-decorated metallophthalocyanines;[256] the Co^{II} version (**25**) was found to be most active when electropolymerized onto glassy carbon, although the overpotential was still quite high at 0.7 V and current densities quite modest at 0.6 mA/cm^2.

5.5.2.2. Model Complexes of Hydrogenase. A burgeoning class of molecular HER catalysts are modeled after nature's proton-reducing enzyme, hydrogenase. Operating very near the thermodynamic potential, hydrogenases catalyze both directions of the H^+/H_2 couple. The electrochemical properties of electrode-adsorbed hydrogenases have been

Chart 2

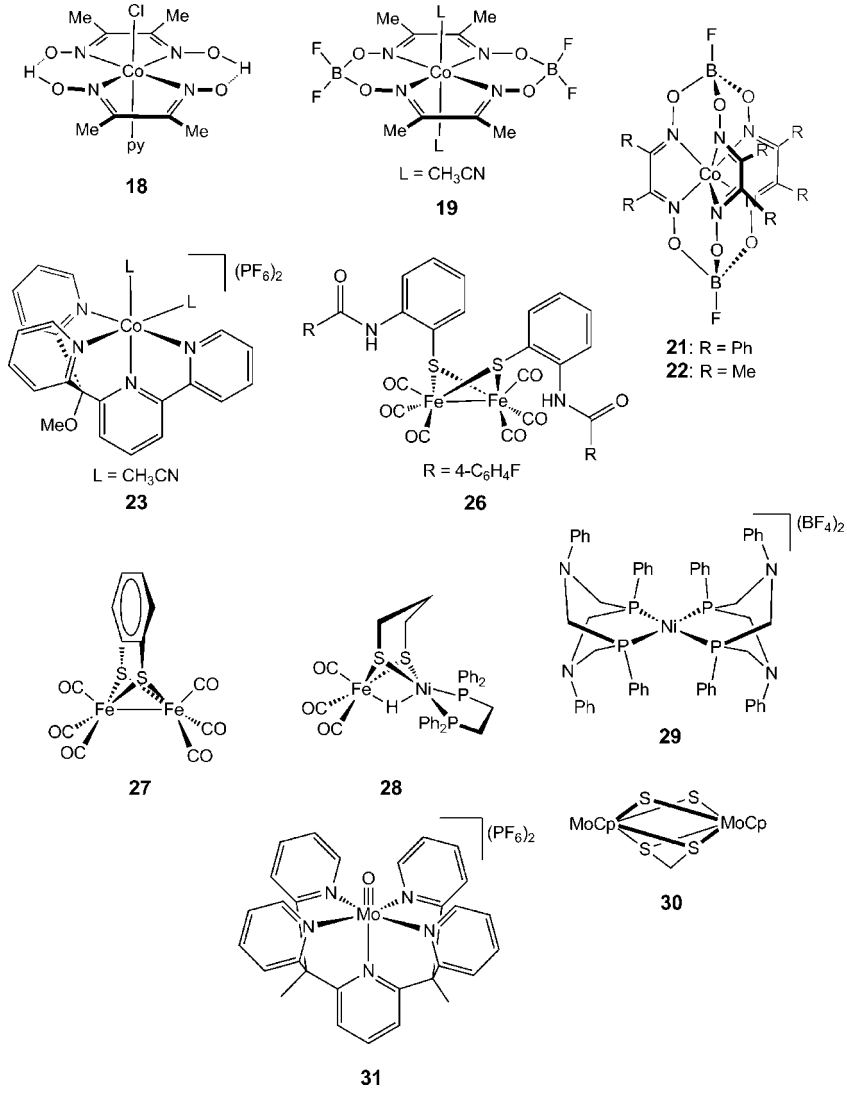

extensively interrogated, and recent reviews summarize many of these experiments.[257,258]

Small-molecule models of the hydrogenase active site are extensively studied as electrocatalysts for proton reduction. The field is extensive, and comprehensive reviews have appeared in recent years.[259−261] Complexes modeled after [Fe]-, [FeFe]-, and [FeNi]-hydrogenase active sites have all been described, although the electrocatalytic properties of the recently emerging [Fe]-hydrogenase models have not been interrogated. [FeFe]-hydrogenase models, frequently featuring two bridging sulfides to mimic the enzyme active site, have been studied extensively as catalysts for proton reduction, exclusively in organic solvents. Tabulated overpotentials range from 0.2 to 2.0 V, most typically in the range of 0.5 to 0.8 V.[260] Catalytic activities likewise show a large range throughout the series of complexes. For example, [μ-S-2-(4-$FC_6H_4CONHC_6H_4$)]$_2$[$Fe_2(CO)_6$] (**26**) has a very good overpotential of 0.2 V but the current enhancements in the presence of acid are quite small.[262] The peak reduction current is augmented by a factor of ca. 1.6 when a 1.0 mM CH_3CN solution of this complex is subjected to 40 mM acetic acid. Conversely, a similar complex, [(μ-1,2-benzenedithiolato)][$Fe_2(CO)_6$] (**27**), shows a current enhancement factor of 32 when 50 mM acetic acid was added to a 1.00 mM CH_3CN solution of the catalyst, although the overpotential in this scenario was much higher at 0.65 V.[263] These preceding examples, although just two of many hydrogenase model complexes, demonstrate that seemingly minor changes in the ligand environment can heavily influence the electrocatalytic properties. [FeFe]-hydrogenase models have been surface-immobilized,[264−266] Although in only one instance are electrocatalytic properties reported,[267] and in this case the electrochemical performance is poor.

Structural models of [NiFe]-hydrogenase complexes are also known. Two reports by Tatsumi and co-workers describe structural models that are thermally unstable, precluding electrochemical characterization,[268,269] and Rauchfuss has described the electrocatalytic proton reduction of dithiolato-bridged [$(CO)_3$Fe(pdt)(μ-H)Ni(dppe)](BF_4) (**28**) (pdt = propanedithiolate, dppe = 1,2-bis(diphenylphosphino)ethane).[270] The complex operates at 0.6 V overpotential, as determined from a cyclic voltammogram of a 1 mM acetonitrile solution in the presence of CF_3COOH. When the acid concentration is 24 mM, the corresponding current density is ca. 0.8 mA/cm^2.

5.5.2.3. Nickel Diphosphine Complexes. Having demonstrated H_2 cleavage by relatively simple Ni(II) diphosphine complexes, DuBois and collaborators have incorporated pendant amine bridges to facilitate proton relay within a square-planar tetraphosphorous coordination environment.[271]

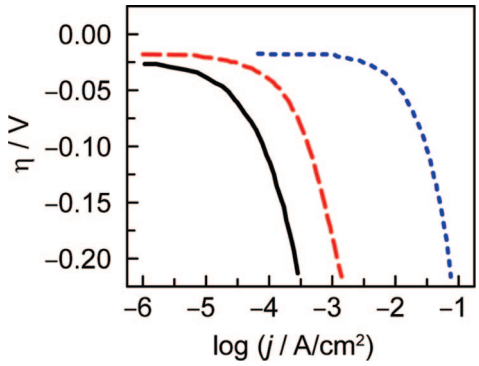

Figure 15. Logarithmic plot showing the applied potential as a function of the current density for a blank electrode containing gas diffusion layer (GDL) on Nafion (black solid line), a MWCNT/GDL electrode functionalized with a derivative of **29** (red long-dashed line), and the rightmost curve (blue dashed line) is that for a commercial membrane electrode assembly (MEA) with highly dispersed platinum (0.5 mg_{Pt}/cm^2). Reprinted with permission from ref 274. Copyright 2009 American Association for the Advancement of Science.

Whereas several of these complexes have been shown to be competent H_2 oxidation catalysts, the complex $[Ni(P_2^{Ph}N_2^{Ph})_2(CH_3CN)](BF_4)_2$ (**29**) ($P_2^{Ph}N_2^{Ph}$ = 1,3,5,7-tetraphenyl-1,5-diaza-3,7-diphospha-cyclooctane) is a representative example of a Ni^{II} HER electrocatalyst. In acetonitrile, this complex catalyzes reduction of triflic acid at 0.6 V overpotential, with a current density of ca. 0.8 mA/cm^2 at that potential when 0.64 mM of the catalyst is in solution with 33.9 mM triflic acid in acetonitrile.[272] The overpotential is considerably smaller, at 0.4 V, when the acid is protonated DMF, which has a pK_a better matched to that of the catalyst.[273] These complexes covalently attached onto multiwalled carbon nanotube (MWCNT) electrodes operate in 0.5 M H_2SO_4,[274] with catalytic onset at very low overpotential. Figure 15 shows that the activity of this catalyst is modest when compared to the unmodified electrode and to Pt.

5.5.2.4. Other Molecular HER Catalysts. Early transition metal HER catalysts are rare. An exception is the Mo_2S_2 dimer capped by cyclopentadienyl rings, $CpMo(\mu\text{-}S)_2S_2CH_2$ (**30**), which reduces protons in acetonitrile solution ($\eta = 120$ mV) when *p*-cyanoanilinium is the acid.[275] The activity of this catalyst can be approximated from the reported bulk electrolysis data. When a 1.1 mM acetonitrile solution of the catalyst is electrolyzed with an applied overpotential of 0.37 V in the presence of 31 mM *p*-cyanoanilinium, an average current of 4.9 mA is observed. The electrolysis was carried out with a vitreous carbon electrode, making an absolute determination of current density difficult.

Another early transition metal HER catalyst, based on a molybdenum-oxo framework and supported by the pentadentate ligand 2,6-bis(1,1-bis(2-pyridyl)ethyl)pyridine (PY5Me2), has been reported to electrocatalyze hydrogen production in neutral water.[276] Some steady-state coulometric data were reported for a solution of 7.7 μM $[(PY5Me_2)MoO](PF_6)_2$ (**31**) in 0.6 M phosphate buffer at pH 7. From this data, a Tafel slope of 65 mV can be estimated between 467 and 617 mV overpotential values, with an extrapolated exchange current density of 0.063 pA/cm^2. A bulk electrolysis on a long time scale showed a stable current value over the course of 71 h, with a current density of ca. 9.1 mA/cm^2 reported at 1 V overpotential.

5.6. Full System Requirements

Water splitting by OER catalysts release oxygen and four protons and four electrons (eq 13, which may be combined at a spatially isolated catalyst to yield H_2 as the solar fuel. The resulting H_2 can be used either directly in a fuel cell[277,278] or combusted directly in an engine.[279] In an indirect solar configuration,[280] electricity produced from a solar photovoltaic (PV) is wired to an electrolyzer, which converts water into hydrogen and oxygen gas. A storage system holds the hydrogen until energy output is required, at which point the hydrogen and (atmospheric) oxygen may be recombined in a fuel cell to produce electricity locally.

A key consideration for any energy storage application involving hydrogen fuel is the amount and conditions of the stored hydrogen. The storage of hydrogen is currently an active area of research, and new materials are being developed to store large amounts of hydrogen in small volumes at low pressures, near-ambient temperatures, and with high energy efficiency for the storage-release cycle.[281,282] For stationary applications where volume is less of a concern, inexpensive storage is afforded by pressurization of hydrogen up to 200−300 bar in simple single-walled containers. Next-generation storage technologies include the addition of hydrogen absorbent materials to the tanks to increase the storage capacity. Examples of such materials include metal hydrides,[282] carbon nanotubes,[281] and metal organic frameworks (MOFs).[283]

The interconversion of one form of energy to another inevitably involves inefficiencies upon each converting step. For the indirect solar fuels scheme, knowledge of the efficiency of each conversion step, along with the overall system efficiency, is critical in comparing fuels to other energy storage technologies. For indirect solar fuels there are three conversions: (1) electricity to fuel (e.g., electrolysis), (2) fuel to stored fuel (e.g., H_2 compression), and (3) stored fuel back to electricity (e.g., fuel cell). The overall system efficiency is determined by the energy losses associated with each of the electrolysis, storage, and fuel cell devices. This cycle contrasts battery technologies in which electricity is stored directly. Approximate efficiencies for each step are 80% for electrolysis, 85% for compression to 200 atm, and 50% for a fuel cell to give an overall storage efficiency of 32% for hydrogen storage as compared to the ∼80% storage efficiency of a battery. Nevertheless, the chemical value and high energy density of fuels demand that they be used as media for energy storage. Fuels will be vital for energy applications that are sensitive to weight (i.e., transportation) and chemical functionality (e.g., ammonia synthesis for fertilizer, natural products synthesis, etc.). Moreover, the direct solar fuels route offers a means to impact the cost of both the solar collection *and* storage, and, in so doing, will impact both the solar collection and storage markets.

5.7. Hydrogen Fixation with Carbon Dioxide to Liquid Fuels

The combination of the four protons and four electrons to yield hydrogen is not the only option for the solar fuel. If the four protons and four electrons released upon water splitting are combined with CO_2, a liquid fuel may be synthesized.[284] It should be noted that CO_2 is not sequestered in a solar fuels cycle (because it is regenerated upon fuels combustion); rather CO_2 is simply a hydrogen carrier. Many of these fuels have improved volumetric energy densities

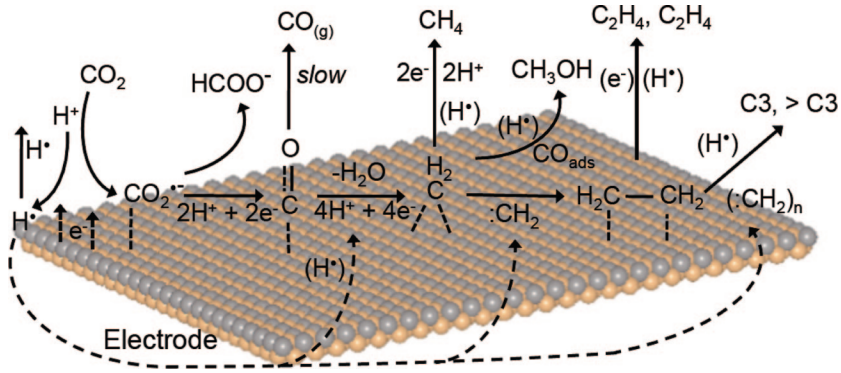

Figure 16. Proton-coupled electron transfer pathways proposed for the reduction of CO_2 at metal electrodes involving various intermediates to form C1 and >C2 fuels. Figure adapted from ref 288. Reproduced by permission of the Royal Society of Chemistry.

compared to hydrogen and thus alleviate many of the challenges associated with hydrogen storage.

There are two prevailing approaches to CO_2 reduction:

(1) CO_2 and H_2O may be converted into syngas (CO and H_2), followed by Fischer−Tropsch chemistry

$$n\mathrm{CO} + 2n\mathrm{H_2} \rightarrow \mathrm{C}_n\mathrm{H}_{2n} + n\mathrm{H_2O} \text{ and}$$
$$n\mathrm{CO} + (2n + 1)\mathrm{H_2} \rightarrow \mathrm{C}_n\mathrm{H}_{2n+2} + n\mathrm{H_2O} \quad (25)$$

to furnish liquid fuels.[285] This approach is well adapted to extremely large centralized elevated temperatures and pressures. The process is in principle scalable, and some work has gone into the fabrication of small-scale reactors, however, FT has yet to be implemented on smaller scales due to the lack of a cheap, distributed form of hydrogen. (2) The conversion of CO_2 directly to liquid fuels via a catalyst driven by the electrical input from a renewable source (indirect) or a catalyst that operates from the wireless current produced by a semiconductor (direct). For either approach, progress on developing catalysts transform CO_2 to C_1 or C_n ($n > 2$) fuels has been slow.[286−288] Most systems developed thus far stop at CO formation, and others have high overpotentials and low turnover numbers or require sacrificial reagents. The primary stumbling block to advances in CO_2 catalysis has been the inability to manage the underlying science needed for CO_2 reduction.

The formation of C−C bonded species requires the multiple proton-coupled electron transfer processes at catalyst active sites needed for C1 reduction and also the reductive coupling of C1 molecules. The two main proton-coupled electron transfer pathways shown in Figure 16 are proposed to be operative at electrode surfaces.[288,289] These pathways involve either molecular chemisorption of CO_2 to then produce C1 oxygenates or dissociative chemisorption and hydrogenation of CO_2 to produce >C2 hydrocarbons. Although conclusive evidence about various pathways for CO_2 electrochemical reaction still is still lacking, CO_2 reduction is sensitive to the electrode surface structure, composition, adsorbed intermediates, pH, and CO_2 concentration.[290] For example, formic acid is the predominant reduction product on Hg, Pb, Sn, and Cd, whereas on Ag, Au, Zn, and Pd electrodes, the product is CO.[291] Almost no reduction of CO_2 takes place on Ti, Mo, Rh, and Pt, with the predominant product being H_2 via the reduction of H_2O.[292] Other products include dimethyl ether and other oxygenates by Fischer−Tropsch type (FT) catalysts involving Fe, Co, and Ni.[293] CO_2 can be reduced to ethylene at a copper electrode with a current density of 2.5 mA cm^{-2} with a Faradaic efficiency of 21.2%.[294,295] More recently, CO_2 has been shown to be reduced to methanol at p-GaP electrode under illumination at 200−300 mV of underpotential and a Faradaic efficiency approaching 100% in the presence of a dissolved pyridinium (pyH^+) mediator.[296]

6. Concluding Remarks

A society powered by solar energy drives inextricably to the heart of delivering the triumvirate of a plentiful, secure, and carbon-neutral energy supply to future generations. The weakest link for the large-scale deployment of solar energy and for that matter, any renewable energy source, is energy storage. Energy storage technology increases the value of all renewable energy supplies whether they are centralized or decentralized. However, centralized (over the grid) or decentralized energy distribution results in different targets for energy storage as a result of different time scales and the nature of the demand. Grid storage is particularly germane to the legacy world, which has inherited a large energy infrastructure. Most grid-based storage mechanisms are mechanical and they span storage needs, with time scales of microseconds to days. The chemical challenges in providing grid-based storage mechanisms are few, largely isolated to the development of batteries and supercapacitors. Of greater pertinence to the chemist are new storage mechanisms for highly distributed renewable energy generation. Novel battery chemistries and engineering will enable safer devices that operate at higher power densities. But as society knows, for large-scale energy storage, chemical fuels are unmatched in terms of their energy density. The challenge to chemistry is to make solar fuels production efficient and low cost. In effecting such chemistry, the solar-driven single electron charge separation of semiconductors must be coupled to the multielectron, multiproton chemistry of solar fuels generation. The critical element for this coupling is a heterogeneous or homogeneous catalyst that is interfaced directly or indirectly (via a photovoltaic) to the semiconductor. The most sustainable source of protons and electrons for solar fuels production is water, which when split by an OER catalyst delivers oxygen and the requisite four electrons and protons needed for fuels production. The electrons and protons may be directly combined to produce H_2 by a HER catalyst or, with future research discovery, combined with CO_2 to furnish a liquid fuel. As described herein, the best OER and HER catalysts are heterogeneous when a normalized comparison of performance is made between homogeneous and heterogeneous catalysts. Notwithstanding, homogeneous catalysts give the most detailed insights into the mechanism of oxygen and hydrogen production. Molecular

catalysts such as Co−Pi, which operate from a heterogeneous phase, unifies the disciplines of homogeneous and heterogeneous catalysis. The Co−Pi catalyst is an exemplar for providing a roadmap of using molecular design principles to create catalysts for real-world energy technologies.[300]

New catalysts to effect solar to fuels conversions are critical research needs to enable an energy independent society of the future. The greatest need for these catalysts is to make highly distributed solar to fuels conversion schemes available to those of the nonlegacy world. If the cost of highly distributed, personalized solar energy can be decreased through discovery, then the development of the nonlegacy world can occur within an energy infrastructure that is of the future and not the past. Considering that it is the 6 billion nonlegacy users that are driving the enormous increase in energy demand by midcentury, a research target of chemistry to deliver personalized solar energy provides the global society its most direct path to providing a solution for its sustainable energy future.

7. References

(1) Energy Information Association; U.S. Department of Energy: Washington DC; www.eia.doe.gov (accessed January 2010).
(2) Lewis, N. S.; Nocera, D. G. *Proc. Natl. Acad. Sci. U.S.A.* **2006**, *103*, 15729.
(3) Hoffert, M. I.; Caldeira, K.; Jain, A. K.; Haites, E. F.; Harvey, L. D. D.; Potter, S. D.; Schlesinger, M. E.; Schneider, S. H.; Watts, R. G.; Wigley, T. M. L.; Wuebbles, D. J. *Nature* **1998**, *395*, 881.
(4) Smalley, R. E. *Mater. Res. Soc. Bull.* **2005**, *30*, 412.
(5) *2009 World Population Data Sheet*; Population Reference Bureau: Washington, DC, 2009; www.prb.org.
(6) Nocera, D. G. *Daedalus* **2006**, *135*, 112.
(7) Abbott, D. *Proc. IEEE* **2010**, *98*, 42.
(8) MacKay, D. J. C. *Sustainable Energy—Without the Hot Air*; UIT Cambridge: Cambridge, UK, 2009.
(9) Bolton, J. R.; Hall, D. O. *Annu. Rev. Energy* **1979**, *4*, 353.
(10) Ansolabehere, S.; Deutch, J.; Driscoll, M.; Gray, P. E; Holdren, J. P.; Joskow, P. L.; Lester, R. K.; Moniz, E. J.; Todreas, N. E. *The Future of Nuclear Power*; MIT Press: Cambridge, MA, 2003.
(11) *Climate Change 2007: Mitigation of Climate Change*; IPCC Working Group III Fourth Assessment Report; Intergovernmental Panel on Climate Change: Geneva, 2007.
(12) Barber, J. *Chem. Soc. Rev.* **2009**, *38*, 185.
(13) Eisenberg, R.; Nocera, D. G. *Inorg. Chem.* **2005**, *44*, 6799.
(14) Curtright, A. E.; Apt, J. *Prog. Photovoltaics* **2008**, *16*, 241.
(15) Jensen, J.; Sorenson, B. *Fundamentals of Energy Storage*; Wiley: New York, 1984.
(16) Tanaka, M. *Energy Policy* **2006**, *34*, 3634.
(17) Collarespereira, M.; Rabl, A. *Solar Energy* **1979**, *22*, 155.
(18) Deutch, J. M. In *Energy Security and Climate Change*; Trilateral Commission, Brookings Institute Press: Washington, DC, 2007.
(19) Yergin, D. *Foreign Affairs* **2006**, *85*, 69.
(20) Nocera, D. G. *ChemSusChem* **2009**, *2*, 387.
(21) Nocera, D. G. *Inorg. Chem.* **2009**, *48*, 10001.
(22) *What Every Engineer Should Know About Manufacturing Cost Estimating*, 2nd ed; Malstrom, E. M., Ed.; John Wiley: New York, 1991.
(23) *Encyclopedia of Production and Manufacturing Management*; Swamidass, P. M., Ed.; Kluwer Academic: Boston, 1995.
(24) Nocera, D. G. *Energy Environ. Sci.* **2010**, *3*, 993.
(25) Chupka, M. W.; Basheda, G. *Rising Utility Construction Costs: Sources and Impacts*; The Brattle Group, Edison Foundation: Washington, DC, 2007.
(26) Green, M. A. *J. Mater. Sci.: Mater. Electron.* **2007**, *18*, S15–S19.
(27) Hegedus, S. *Prog. Photovoltaics* **2006**, *14*, 393.
(28) Goetzberger, A.; Hebling, C.; Schock, H. W. *Mater. Sci. Eng., R* **2003**, *40*, 1.
(29) Shaheen, S. E.; Ginley, D. S.; Jabbour, G. E. *Mater. Res. Soc. Bull.* **2005**, *30*, 10.
(30) Brabec, C. J.; Sariciftci, N. S.; Hummelen, J. C. *Adv. Funct. Mater.* **2001**, *11*, 15.
(31) Gunes, S.; Neugebauer, H.; Sariciftci, N. S. *Chem. Rev.* **2007**, *107*, 1324.
(32) Brabec, C. J. *Solar Energy Mater. Solar Cells* **2004**, *83*, 273.
(33) Grätzel, M. *Nature* **2001**, *414*, 338.
(34) *Thin Film Photovoltaics Markets: 2008 and Beyond*; Report Nano-054; NanoMarkets: Glen Allen, VA, 2008.
(35) Ginley, D.; Green, M. A.; Collins, R. *Mater. Res. Soc. Bull.* **2008**, *33*, 355.
(36) Bredas, J.-L.; Durrant, J. R. *Acc. Chem. Res.* **2009**, *42*, 1689.
(37) Ruttinger, W.; Dismukes, G. C. *Chem. Rev.* **1997**, *97*, 1.
(38) Yagi, M.; Kaneko, M. *Chem. Rev.* **2001**, *101*, 21.
(39) McEvoy, J. P.; Brudvig, G. W. *Chem. Rev.* **2006**, *106*, 4455.
(40) Eisenberg, R.; Gray, H. B. *Inorg. Chem.* **2008**, *47*, 1697.
(41) Esswein, A. J.; Nocera, D. G. *Chem. Rev.* **2007**, *107*, 4022.
(42) Tard, C.; Pickett, C. J. *Chem. Rev.* **2009**, *109*, 2245.
(43) Eisenberg, R.; Nocera, D. G. *Inorg. Chem.* **2005**, *44*, 6799.
(44) Hammarström, L.; Hammes-Schiffer, S. *Acc. Chem. Res.* **2009**, *42*, 1859.
(45) Savéant, J.-M. *Chem. Rev.* **2008**, *108*, 2348.
(46) Bottling Electricity: Storage as a Strategic Tool for Managing Variability and Capacity Concerns in the Modern Grid; DOE Electricity Advisory Council: Washington, DC, December, 2008; http://oe.energy.gov/eac.htm.
(47) Tester, J. W.; Drake, E. M.; Golay, W. W.; Driscoll, M. J.; Peters, W. A.; *Sustainable Energy*; MIT Press: Cambridge, MA, 2005, Chapter 16.
(48) Boes, E. L.; Goldstein, L.; Nix, G. Energy Storage and Overview; National Renewable Energy Laboratory Report; U.S. Department of Energy: Washington, DC, 2000.
(49) Pickard, W. F.; Shen, A. Q.; Hansing, N. J. *Renew. Sustain. Energy Rev.* **2009**, *13*, 1934.
(50) Ibrahima, H.; Ilincaa, A.; Perron, J. *Renewable Sustainable Energy Rev.* **2008**, *12*, 1221.
(51) Linden, S.v. d. *Energy* **2006**, *31*, 3446.
(52) Dell, R. M.; Rand, D. A. J. *J. Power Sources* **2001**, *100*, 2.
(53) Smith, S. C.; Sen, P. K. Advancement of Energy Storage Devices and Applications in Electrical Power System; IEEE Xplore, http://ieeexplore.ieee.org/stamp/stamp.jsp?arnumber=04596436(accessed November 2009).
(54) Hydroelectric; Energy Information Administration, U.S Department of Energy, http://www.eia.doe.gov/cneaf/solar.renewables/page/hydroelec/hydroelec.html (accessed September 2009).
(55) 2007 Survey of Energy Resources; World Energy Council: London, 2007; Executive Summary http://www.world-energy.org/documents/ser2007_executive_summary.pdf (accessed December 2009).
(56) Key World Energy Statistics 2007; International Energy Agency (IEA): Paris, 2007; http://www.iea.org/textbase/nppdf/free/2007/key_stats_2007.pdf (accessed December 2009).
(57) Glasnovic, Z.; Margeta, J. *Renewable Energy* **2009**, *34*, 1742.
(58) Jacobson, M. Z. *Energy Environ. Sci.* **2009**, *2*, 148.
(59) Leonard, W.; GrobeM. Sustainable Electrical Energy Supply with Wind and Pumped Storage—A Realistic Long-term Strategy or Utopia; General Meeting Report; IEEE Power and Energy Society: Piscataway, NJ, 2004; p 1221.
(60) Bueno, C.; Carta, J. A. *Renewable Sustainable Energy Rev.* **2006**, *10*, 312.
(61) Peltier, R. *Power* **2006**, *150*, 54.
(62) Kakue, T.; Saito, M. *Int. Water Power Dam Construct.* **2006**, *58*, 36.
(63) *Micro Hydroelectric Systems*; http://www.oregon.gov/ENERGY/RENEW/Hydro/Hydro_index.shtml (accessed December 2009).
(64) Scott, F. M. *Energy* **1977**, *2*, 20.
(65) Tam, S. W.; Blomquist, C. A.; Kartsounes, G. T. *Energy Sources* **1979**, *4*, 329.
(66) Uddin, N.; Asce, M. *Geotech. Geol. Eng.* **2003**, *21*, 331.
(67) Denholm, P. *Renewable Energy* **2006**, *31*, 1355.
(68) Atkins, P. *Physical Chemistry*, 6th ed.; Freeman: New York, 1998.
(69) Denholm, P.; Kulcinski, G. L.; Holloway, T. *Environ. Sci. Technol.* **2005**, *39*, 1903.
(70) Hounslow, D. R.; Grindley, W.; Loughlin, R. M.; Daly, J. *J. Eng. Gas Turbines Power* **1998**, *120*, 875.
(71) Bolund, B.; Bernhoff, H.; Leijon, M. *Renewable Sustainable Energy Rev.* **2007**, *11*, 235.
(72) Ruddell, A. *Investigation on Storage Technologies for Intermittent Renewable Energies: Evaluation and Recommended R&D Strategy*; Ivestire-Network Storage Technology Report WP-ST6: Flywheels, **2003**.
(73) de Andrade, R.; Sotelo, G. G.; Ferreira, A. C.; Rolim, L. G. B.; da Silva Neto, J. L.; Stephan, R. M.; Suemitsu, W. I.; Nicolsky, R. *IEEE Trans. Appl. Supercond.* **2007**, *17*, 2154.
(74) Hull, J. R. *Rep. Prog. Phys.* **2003**, *66*, 1865.
(75) Lazarewicz, M. *Flywheel Based Frequency Regulation Pilot Projects*; Proceedings of the Annual Meeting of the Electricity Storage Association, Toronto, Canada, 2005.
(76) Emissions Comparison for a 20 MW Flywheel-Based Frequency Regulation Power Plant; Sandia National Laboratories, KEMA Albuquerque, NM, 2007.

(77) Luongo, C. A. *IEEE Trans. Magn.* **1996**, *32*, 2214.
(78) Xue, X. D.; Cheng, F. E. W.; Sutanto, D. *Supercond. Sci. Technol.* **2006**, *19*, R31–R39.
(79) Tosaka, T.; Koyanagi, K.; Ohsemochi, K.; Takahashi, M.; Ishii, Y.; Ono, M.; Ogata, H.; Nakamoto, K.; Takigami, H.; Nomura, S.; Kidoguchi, K.; Onoda, H.; Hirano, N.; Nagaya, S. *IEEE Trans. Appl. Supercond.* **2007**, *17*, 2010.
(80) Loyd, R. J.; Schoenung, S. M.; Nakamura, T.; Hassenzahl, W. V.; Rogers, J. D.; Purcell, J. R.; Lieurance, D. W.; Hilal, M. A. *IEEE Trans. Magn.* **1987**, *23*, 1323.
(81) Hassenzahl, W. V.; Hazelton, D. W.; Johnson, B. K.; Komarek, P.; Noe, M.; Reis, C. T. *Proc. IEEE* **2004**, *92*, 1655.
(82) *Liquid Battery*; Technology Review, MIT Press: Cambridge, MA, 2009; p 46.
(83) Hamlen, R. P.; Atwater, T. B. in *Handbook of Batteries*, 3rd ed.; Linden, D.; Reddy, T. B., Eds.; McGraw-Hill; New York, 2002.
(84) Girishkumar, G.; McCloskey, B.; Luntz, A. C.; Swanson, S.; Wilcke, W. *J. Phys. Chem. Lett.* **2010**, *1*, 2193.
(85) Bruce, P. G.; Scrosati, B.; Tarascon, J. M. *Angew. Chem., Int. Ed.* **2008**, *47*, 29.
(86) Technology and Applied R&D Needs for Electrical Energy Storage; A Resource Document for Basic Research Needs for Electrical Energy Storage; U.S. Department of Energy: Washington, DC, 2007.
(87) Palaćin, M. R. *Chem. Soc. Rev.* **2009**, *38*, 2565.
(88) Dell, R. M.; Rand, D. A. J. *Understanding Batteries*; Royal Society of Chemistry: Cambridge, UK, 2001.
(89) Flipsen, S. F. J. *J. Power Sources* **2006**, *162*, 927.
(90) Linden, D.; Reddy, T. B., Eds.; *Handbook of Batteries*, 3rd ed.; McGraw-Hill: New York, 2002.
(91) Shukla, A. K.; Venugopalan, S.; Hariprakash, B. *J. Power Sources* **2001**, *100*, 125.
(92) Ritchie, A.; Howard, W. *J. Power Sources* **2006**, *162*, 809.
(93) Sudworth, J. L. *J. Power Sources* **1984**, *11*, 143.
(94) Ponce de León, C.; Frías-Ferrer, A.; González-García, J.; Szánto, D. A.; Walsh, F. C. *J. Power Sources* **2006**, *160*, 716.
(95) Lu, Y.-C.; Gasteiger, H. A.; Parent, M. C.; Chiloyan, V.; Shao-Horn, Y. *Electrochem. Solid State Lett.* **2010**, *13*, A69.
(96) Chakkaravarthy, C.; Abdul Waheed, A. K.; Udupa, H. V. K. *J. Power Sources* **1981**, *6*, 203.
(97) Bullar, G. L.; Sierra-Alcazar, H. B.; Lee, H. L.; Morris, J. L. *IEEE Trans. Magn.* **1989**, *25*, 102.
(98) Conway, B. E. *Electrochemical Supercapacitors*; Kluwer Academic Plenum: New York, 1999.
(99) Miller, J. R.; Simon, P. *Science* **2008**, *321*, 651.
(100) Simon, P.; Gogotsi, Y. *Nature Mater.* **2008**, *7*, 845.
(101) Simon, P.; Gogotsi, Y. *Philos. Trans. R. Soc., A* **2010**, *368*, 3457.
(102) Barton, J. P.; Infield, D. G. *IEEE Trans. Energy Convers.* **2004**, *19*, 441.
(103) Winter, M.; Brodd, R. J. *Chem. Rev.* **2004**, *104*, 4245.
(104) Zhong, D. K.; Sun, J.; Inumaru, H.; Gamelin, D. R. *J. Am. Chem. Soc.* **2009**, *131*, 6086.
(105) Zhong, D. K.; Gamelin, D. R. *J. Am. Chem. Soc.* **2010**, *132*, 4202.
(106) Steinmiller, E. M. P.; Choi, K. S. *Proc. Natl. Acad. Sci. U.S.A.* **2009**, *106*, 20633.
(107) Tafel, J. *Z. Phys. Chem.* **1905**, *50*, 641.
(108) Burstein, G. T. *Corros. Sci.* **2005**, *47*, 2858.
(109) Conway, B. E.; Bai, L.; Sattar, M. A. *Int. J. Hydrogen Energy* **1987**, *9*, 607.
(110) Matsumoto, Y.; Sato, E. *Mater. Chem. Phys.* **1986**, *14*, 397.
(111) Hoare, J. P. In *Encyclopedia of Electrochemistry of the Elements*; Bard, A. J., Ed.; Marcel Dekker: New York, 1982; Vol. 2, p 191.
(112) Hoare, J. P. *Electrochemistry of Oxygen*; Interscience: New York, 1968; p 81.
(113) Trasatti, S. In *Electrochemistry of Novel Materials*; Lipkowski, J., Ross, P. N., Ed.; VCH: New York, 1994; p 207.
(114) Damjanovic, A.; Dey, A.; Bockris, J. O'M *Electrochim. Acta* **1966**, *11*, 791.
(115) Appleby, A. J. *J. Electroanal. Chem.* **1970**, *24*, 97.
(116) Gottesfeld, S.; Srinivasan, S. *J. Electroanal. Chem.* **1978**, *86*, 89.
(117) Conway, B. E.; Tilak, B. V. In *Advances in Catalysis*; Eley, D. D., Pines, H., Weisz, P. B., Ed.; Academic Press: New York, 1992; Vol. 38, p 18.
(118) Rossmeisl, J.; Logadottir, A.; Nørskov, J. K. *Chem. Phys.* **2005**, *319*, 178.
(119) Bockris, J. O'M.; Otagawa, T. *J. Phys. Chem.* **1983**, *87*, 2960−.
(120) Bockris, J. O'M.; Otagawa, T. *J. Electrochem. Soc.* **1984**, *131*, 290.
(121) Trasatti, S. *Electrochim. Acta* **1984**, *29*, 1503.
(122) Rasiyah, P.; Tseung, A. C. C. *J. Electrochem. Soc.* **1984**, *131*, 803.
(123) Rossmeisl, J.; Qu, Z.-W.; Zhu, H.; Kroes, G.-J.; Nørskov, J. K. *J. Electroanal. Chem.* **2007**, *607*, 83.
(124) Jasem, S. M.; Tseung, A. C. C. *J. Electrochem. Soc.* **1979**, *126*, 1353.
(125) Kibria, A. K. M. F.; Tarafdar, S. A. *Int. J. Hydrogen Energy* **2002**, *27*, 879.
(126) Singh, R. N.; Madhu; Awasthi, R.; Sinha, A. S. K. *Electrochim. Acta* **2009**, *54*, 3020−.
(127) Singh, R. N.; Madhu; Awasthi, R.; Tiwari, S. K. *Int. J. Hydrogen Energy* **2009**, *34*, 4693−.
(128) Singh, R. N.; Pandey, J. P.; Singh, N. K.; Lal, B.; Chartier, P.; Koenig, J.-F. *Electrochim. Acta* **2000**, *45*, 1911.
(129) Singh, R. N.; Singh, N. K.; Singh, J. P. *Electrochim. Acta* **2002**, *47*, 3873.
(130) MacDonald, J. J.; Conway, B. E. *Proc. R. Soc. London, A* **1962**, *269*, 419.
(131) Lyons, M. E. G.; Brandon, M. P. *Int. J. Electrochem. Sci.* **2008**, *3*, 1425.
(132) Damjanovic, A.; Jovanovic, B. *J. Electrochem. Soc.* **1976**, *123*, 374.
(133) Choquette, Y.; Ménard, H.; Brossard, L. *Int. J. Hydrogen Energy* **1990**, *15*, 21.
(134) Therese, G. H. A.; Kamath, P. V. *Chem. Mater.* **2000**, *12*, 1195.
(135) Spataru, N.; Terashima, C.; Tokuhiro, K.; Sutanto, I.; Tryk, D. A.; Park, S.-M.; Fujishima, A. *J. Electrochem. Soc.* **2003**, *150*, E337−E341.
(136) Nakagawa, T.; Beasley, C. A.; Murray, R. W. *J. Phys. Chem. C* **2009**, *113*, 12958.
(137) Esswein, A. J.; McMurdo, M. J.; Ross, P. N.; Bell, A. T.; Tilley, T. D. *J. Phys. Chem. C* **2009**, *113*, 15068.
(138) Grimes, C. A.; Varghese, O. K.; Ranjan, S. *Light, Water, Hydrogen: The Solar Generation of Hydrogen by Water Photoelectrolysis*; Springer: New York, 2008.
(139) Turner, J. A. *Science* **1999**, *285*, 687.
(140) Lutterman, D. A.; Surendranath, Y.; Nocera, D. G. *J. Am. Chem. Soc.* **2009**, *131*, 3838.
(141) Kanan, M. W.; Nocera, D. G. *Science* **2008**, *321*, 1072.
(142) Dincă, M.; Surendranath, Y.; Nocera, D. G. *Proc. Natl. Acad. Sci. U.S.A.* **2010**, *107*, 10337.
(143) Surendranath, Y.; Dincă, M.; Nocera, D. G. *J. Am. Chem. Soc.* **2009**, *131*, 2615.
(144) Kanan, M. W.; Surendranath, Y.; Nocera, D. G. *Chem. Soc. Rev.* **2009**, *38*, 109.
(145) Nocera, D. G. *ChemSusChem* **2009**, *2*, 387.
(146) Burke, L. D.; Murphy, O. J.; O'Neill, J. F.; Venkatesan, S.; Schuldiner, S. *J. Chem. Soc., Faraday Trans.* **1977**, *73*, 1659−.
(147) Hu, J.-M.; Zhang, J.-Q.; Cao, C.-N. *Int. J. Hydrogen Energy* **2004**, *29*, 791.
(148) Singh, R. N.; Koenig, J.-F.; Poillerat, G.; Chartier, P. *J. Electrochem. Soc.* **1990**, *137*, 1408.
(149) McEvoy, J. P; Brudvig, G. W. *Chem. Rev.* **2006**, *106*, 4455.
(150) Siegbahn, P. E. M. *J. Am. Chem. Soc.* **2009**, *131*, 18238.
(151) *CRC Handbook of Chemistry and Physics*, 86th ed.; Lide, D. R., Ed.; CRC Publishing: Boca Raton, FL, 2005; pp 8.
(152) Dismukes, G. C.; Brimblecombe, R.; Felton, G. A. N.; Pryadun, R. S.; Sheats, J. E.; Spiccia, L.; Swiegers, G. F. *Acc. Chem. Res.* **2009**, *42*, 1935.
(153) Hurst, J. K. *Coord. Chem. Rev.* **2005**, *249*, 313.
(154) Concepcion, J. J.; Jurss, J. W.; Brennaman, M. K.; Hoertz, P. G.; Patrocinio, A. O. T.; Iha, N. Y. M.; Templeton, J. L.; Meyer, T. J. *Acc. Chem. Res.* **2009**, *42*, 1954.
(155) Brimblecombe, R.; Dismukes, G. C.; Swiegers, G. F.; Spiccia, L. *Dalton Trans.* **2009**, 9374.
(156) Yagi, M.; Kaneko, M. *Chem. Rev.* **2001**, *101*, 21.
(157) Gersten, S. W.; Samuels, G. J.; Meyer, T. J. *J. Am. Chem. Soc.* **1982**, *104*, 4030.
(158) Ellis, C. D.; Gilbert, J. A.; Murphy, W. R., Jr.; Meyer, T. J. *J. Am. Chem. Soc.* **1983**, *105*, 4842−.
(159) Gilbert, J. A.; Eggleston, D. S.; Murphy, W. R., Jr.; Geselowitz, D. A.; Gersten, S. W.; Hodgson, D. J.; Meyer, T. J. *J. Am. Chem. Soc.* **1985**, *107*, 3855−.
(160) Hurst, J. K.; Zhou, J.; Lei, Y. *Inorg. Chem.* **1992**, *31*, 1010.
(161) Lei, Y.; Hurst, J. K. *Inorg. Chem.* **1994**, *33*, 4460.
(162) Chronister, C. W.; Binstead, R. A.; Ni, J.; Meyer, T. J. *Inorg. Chem.* **1997**, *36*, 3814.
(163) Yamada, H.; Hurst, J. K. *J. Am. Chem. Soc.* **2000**, *122*, 5303.
(164) Binstead, R. A.; Chronister, C. W.; Ni, J.; Hartshorn, C. M.; Meyer, T. J. *J. Am. Chem. Soc.* **2000**, *122*, 8464.
(165) Cape, J. L.; Hurst, J. K. *J. Am. Chem. Soc.* **2008**, *130*, 827.
(166) Liu, F.; Concepcion, J. J.; Jurss, J. W.; Cardolaccia, T.; Templeton, J. L.; Meyer, T. J. *Inorg. Chem.* **2008**, *47*, 1727.
(167) Cape, J. L.; Siems, W. F.; Hurst, J. K. *Inorg. Chem.* **2009**, *48*, 8729.
(168) Kinoshita, K.; Yagi, M.; Kaneko, M. *J. Mol. Catal. A: Chem.* **1999**, *142*, 1.
(169) Yagi, M.; Yamaguchi, T.; Kaneko, M. *J. Mol. Catal. A: Chem.* **1999**, *149*, 289.
(170) Nagoshi, K.; Yagi, M.; Kaneko, M. *Bull. Chem. Soc. Jpn.* **2000**, *73*, 2193.
(171) Shiroishi, H.; Yamashita, S.; Kinoshita, K.; Kaneko, M. *Polym. J.* **1999**, *31*, 1175.

(172) Yagi, M.; Kinoshita, K.; Kaneko, M. *J. Phys. Chem.* **1996**, *100*, 11098.
(173) Kinoshita, K.; Yagi, M.; Kaneko, M. *Macromolecules* **1998**, *31*, 6042.
(174) Yagi, M.; Kinoshita, K.; Kaneko, M. *J. Phys. Chem. B* **1997**, *101*, 3957.
(175) Ogino, O.; Nagoshi, K.; Yagi, M.; Kaneko, M. *J. Chem. Soc., Faraday Trans.* **1996**, *92*, 3431.
(176) Yagi, M.; Takano, E.; Kaneko, M. *Electrochim. Acta* **1999**, *44*, 2493.
(177) Petach, H. H.; Elliott, C. M. *J. Electrochem. Soc.* **1992**, *139*, 2217.
(178) Liu, F.; Cardolaccia, T.; Hornstein, B. J.; Schoonover, J. R.; Meyer, T. J. *J. Am. Chem. Soc.* **2007**, *129*, 2246.
(179) Mola, J.; Mas-Marza, E.; Sala, X.; Romero, I.; Rodríguez, M.; Viñas, C.; Parella, T.; Llobet, A. *Angew. Chem., Int. Ed.* **2008**, *47*, 5830.
(180) Wada, T.; Tsuge, K.; Tanaka, K. *Angew. Chem., Int. Ed.* **2000**, *39*, 1479.
(181) Wada, T.; Tsuge, K.; Tanaka, K. *Inorg. Chem.* **2001**, *40*, 329.
(182) Concepcion, J. J.; Jurss, J. W.; Templeton, J. L.; Meyer, T. J. *J. Am. Chem. Soc.* **2008**, *130*, 16462.
(183) Concepcion, J. J.; Jurss, J. W.; Norris, M. R.; Chen, Z.; Templeton, J. L.; Meyer, T. J. *Inorg. Chem.* **2010**, *49*, 1277.
(184) Chen, Z.; Concepcion, J. J.; Jurss, J. W.; Meyer, T. J. *J. Am. Chem. Soc.* **2009**, *131*, 15580.
(185) Brimblecombe, R.; Swiegers, G. F.; Dismukes, G. C.; Spiccia, L. *Angew. Chem., Int. Ed.* **2008**, *47*, 7335.
(186) Howells, A. R.; Sankarraj, A.; Shannon, C. *J. Am. Chem. Soc.* **2004**, *126*, 12258.
(187) Sartorel, A.; Miró, P.; Salvaodori, E.; Romain, S.; Carraro, M.; Scorrano, G.; Di Valentin, M.; Llobet, A.; Bo, C.; Bonchio, M. *J. Am. Chem. Soc.* **2009**, *131*, 16051.
(188) Geletii, Y. V.; Botar, B.; Kögerler, P.; Hillesheim, D. A.; Musaev, D. G.; Hill, C. L. *Angew. Chem., Int. Ed.* **2008**, *47*, 3896−.
(189) Geletii, Y. V.; Besson, C.; Hou, Y.; Yin, Q.; Musaev, D. G.; Quiñonero, D.; Cao, R.; Hardcastle, K. I.; Proust, A.; Kögerler, P.; Hill, C. L. *J. Am. Chem. Soc.* **2009**, *131*, 17360−.
(190) Yin, Q.; Tan, J. M.; Besson, C.; Geletti, Y. V.; Musaev, D. G.; Kuznetsov, A. E.; Luo, Z.; Hardcastle, K. I.; Hill, C. L. *Science* **2010**, *328*, 342.
(191) McDaniel, N. D.; Coughlin, F. J.; Tinker, L. L.; Bernhard, S. *J. Am. Chem. Soc.* **2008**, *130*, 210.
(192) Hull, J. F.; Balcells, D.; Blakemore, J. D.; Incarvito, C. D.; Eisenstein, O.; Brudvig, G. W.; Crabtree, R. H. *J. Am. Chem. Soc.* **2009**, *131*, 8730.
(193) Nakagawa, T.; Bjorge, N. S.; Murray, R. W. *J. Am. Chem. Soc.* **2009**, *131*, 15578.
(194) Rosenthal, J.; Nocera, D. G. *Acc. Chem. Res.* **2007**, *40*, 543.
(195) Rosenthal, J.; Nocera, D. G. *Prog. Inorg. Chem.* **2007**, *55*, 483.
(196) Naruta, Y.; Sasayama, M.; Sasaki, T. *Angew. Chem., Int. Ed. Engl.* **1994**, *33*, 1839.
(197) Gao, Y.; Liu, J. H.; Wang, M.; Na, Y.; Akermark, B.; Sun, L. C. *Tetrahedron* **2007**, *63*, 1987.
(198) Gao, Y.; Akermark, T.; Liu, J. H.; Sun, L. C.; Akermark, B. *J. Am. Chem. Soc.* **2009**, *131*, 8726.
(199) Takada, K.; Fukuda, K.; Osada, M.; Nakai, I.; Izumi, F.; Dilanian, R. A.; Kato, K.; Takata, M.; Sakurai, H.; Takayama-Muromachi, E.; Sasaki, T. *J. Mater. Chem.* **2004**, *14*, 1448.
(200) Sakurai, H.; Tsujii, N.; Suzuki, O.; Kitazawa, H.; Kido, G.; Takada, K.; Sasaki, T.; Takayama-Muromachi, E. *Phys. Rev. B* **2006**, *74*, 092502/1−4.
(201) Sakurai, H.; Osada, M.; Takayama-Muromachi, E. *Chem. Mater.* **2007**, *19*, 6073.
(202) Ren, Z.; Luo, J.; Xu, Z.; Cao, G. *Chem. Mater.* **2007**, *19*, 4432.
(203) Appleby, A. J.; Kita, H; Chemla, M.; Bronoël, G. In *Encyclopedia of Electrochemistry of the Elements*; Bard, A. J., Ed.; Marcel Dekker: New York, 1982; Vol. 9, part A, pp 413.
(204) Tilak, B. V.; Ramamurthy, A. C.; Conway, B. E. *Proc. Indian Acad. Sci.* **1986**, *97*, 359.
(205) Conway, B. E.; Tilak, B. V. *Electrochim. Acta* **2002**, *47*, 3571.
(206) Trasatti, S. *J. Electroanal. Chem.* **1972**, *39*, 163.
(207) Gerischer, H. *Bull. Soc. Chim. Belg.* **1958**, *67*, 506.
(208) Parsons, R. *Trans. Faraday Soc.* **1958**, *54*, 1053.
(209) Sabatier, P. *Ber. Dtsch. Chem. Ges.* **1911**, *44*, 1984.
(210) Nørskov, J. K.; Bligaard, T.; Logadottir, A.; Kitchin, J. R.; Chen, J. G.; Pandelov, S.; Stimming, U. *J. Electrochem. Soc.* **2005**, *152*, J23–J26.
(211) Conway, B. E.; Bai, L.; Sattar, M. A. *Int. J. Hydrogen Energy* **1987**, *9*, 607.
(212) Petrii, O. A.; Tsirlina, G. A. *Electrochim. Acta* **1994**, *39*, 1739.
(213) Bockris, J. O'M.; Potter, E. C. *J. Chem. Phys.* **1952**, *20*, 614.
(214) Bockris, J.O'M.; Potter, E. C. *J. Electrochem. Soc.* **1952**, *99*, 169.
(215) Bockris, J. O'M.; Srinivasan, S. *Electrochim. Acta* **1964**, *9*, 31.
(216) Jakšić, M. M. *Int. J. Hydrogen Energy* **2001**, *26*, 559.
(217) Jakšić, M. M. *Electrochim. Acta* **2000**, *45*, 4085.
(218) Krstajić, N. V.; Grgur, B. N.; Mladenović, N. S.; Vojnović, M. V.; Jakšić, M. M. *Electrochim. Acta* **1997**, *42*, 323−.
(219) Brown, D. E.; Mahmood, M. N.; Man, M. C. M.; Turner, A. K. *Electrochim. Acta* **1984**, *29*, 1551.
(220) Hu, W.; Cao, X.; Wang, F.; Zhang, Y. *Int. J. Hydrogen Energy* **1997**, *22*, 621.
(221) Krstajić, N.; Popov, K.; Spasojević, M.; Atanasoski, R. *J. Appl. Electrochem.* **1982**, *12*, 435.
(222) Stojić, D. L.; Maksić, A. D.; Kaninski, M. P. M.; Cekić, B. D.; Miljanić, S. S. *J. Power Sources* **2005**, *145*, 278.
(223) Hinnemann, B.; Moses, P. G.; Bonde, J.; Jørgensen, K. P.; Nielsen, J. H.; Horch, S.; Chorkendorff, I.; Nørskov, J. K. *J. Am. Chem. Soc.* **2005**, *127*, 5308−.
(224) McEvoy, A. J.; Grätzel, M. *J. Electroanal. Chem.* **1986**, *209*, 391.
(225) Savadogo, O. *J. Electrochem. Soc.* **1992**, *139*, 1082.
(226) Savadogo, O.; Lavoie, H. *Int. J. Hydrogen Energy* **1992**, *17*, 473.
(227) Savadogo, O.; Amuzgar, K.; Piron, D. L. *Int. J. Hydrogen Energy* **1990**, *15*, 783.
(228) Savadogo, O.; Carrier, F.; Forget, E. *Int. J. Hydrogen Energy* **1994**, *19*, 429.
(229) Endoh, E.; Otouma, H.; Morimoto, T.; Oda, Y. *Int. J. Hydrogen Energy* **1987**, *12*, 473.
(230) Raney, M. Finely Divided Nickel. U.S. Patent 1628190, 1927.
(231) Cheong, A. K.; Lasia, A.; Lessard, J. *J. Electrochem. Soc.* **1993**, *140*, 2721.
(232) Shervedoni, R. K.; Lasia, A. *J. Electrochem. Soc.* **1998**, *145*, 2219.
(233) Schuldiner, S. *J. Electrochem. Soc.* **1959**, *106*, 891.
(234) Chen, L.; Guay, D.; Lasia, A. *J. Electrochem. Soc.* **1996**, *143*, 3576.
(235) Ammar, I. A.; Darwish, S. *J. Phys. Chem.* **1959**, *63*, 983.
(236) Shamsul Huq, A. K. M.; Rosenberg, A. J. *J. Electrochem. Soc.* **1964**, *111*, 270.
(237) Bélanger, A.; Vijh, A. K. *J. Electrochem. Soc.* **1974**, *121*, 225.
(238) Pentland, N.; Bockris, J. O'M.; Sheldon, E. *J. Electrochem. Soc.* **1957**, *104*, 182.
(239) Vijh, A. K. *J. Phys. Chem.* **1968**, *72*, 1148.
(240) Felton, G. A. N.; Glass, R. S.; Lichtenberger, D. L.; Evans, D. H. *Inorg. Chem.* **2006**, *45*, 9181.
(241) Fisher, B.; Eisenberg, R. *J. Am. Chem. Soc.* **1980**, *102*, 7361.
(242) Collin, J.-P.; Abdelaziz, J.; Sauvage, J.-P. *Inorg. Chem.* **1988**, *27*, 1986.
(243) Bernhardt, P. V.; Jones, L. A. *Inorg. Chem.* **1999**, *38*, 5086.
(244) Connolly, P.; Espenson, J. H. *Inorg. Chem.* **1986**, *25*, 2684.
(245) Razavet, M.; Artero, V.; Fontecave, M. *Inorg. Chem.* **2005**, *44*, 4786.
(246) Hu, X.; Cossairt, B. M.; Brunschwig, B. S.; Lewis, N. S.; Peters, J. C. *Chem. Commun.* **2005**, 4723.
(247) Hu, X.; Brunschwig, B. S.; Peters, J. C. *J. Am. Chem. Soc.* **2007**, *129*, 8988.
(248) Jacques, P.-A.; Artero, V.; Pécaut, J.; Fontecave, M. *Proc. Natl. Acad. Sci. U.S.A.* **2009**, *106*, 20627.
(249) Baffert, C.; Artero, V.; Fontecave, M. *Inorg. Chem.* **2007**, *46*, 1817.
(250) Berben, L.; Peters, J. C. *Chem. Commun.* **2010**, 398.
(251) Pantani, O.; Naksar, S.; Guillot, R.; Millet, P.; Anxolabéhère-Mallart, E.; Aukauloo, A. *Angew. Chem., Int. Ed.* **2008**, *47*, 9948.
(252) Bigi, J. P.; Hanna, T. E.; Harman, W. H.; Chang, A.; Chang, C. J. *Chem. Commun.* **2010**, 958.
(253) Kellet, R. M.; Spiro, T. G. *Inorg. Chem.* **1985**, *24*, 2373.
(254) Kellet, R. M.; Spiro, T. G. *Inorg. Chem.* **1985**, *24*, 2378.
(255) Knoll, J.; Swavey, S. *Inorg. Chim. Acta* **2009**, *362*, 2989.
(256) Osmanbaş, Ö. A.; Koca, A.; Kandaz, M.; Karaca, F. *Int. J. Hydrogen Energy* **2008**, *33*, 3281.
(257) Vincent, K. A.; Parkin, A.; Armstrong, F. A. *Chem. Rev.* **2007**, *107*, 4366.
(258) Cracknell, J. A.; Vincent, K. A.; Armstrong, F. A. *Chem. Rev.* **2008**, *108*, 2439.
(259) Tard, C.; Pickett, C. J. *Chem. Rev.* **2009**, *109*, 2245.
(260) Felton, G. A. N.; Mebi, C. A.; Petro, B. J.; Vannucci, A. K.; Evans, D. H.; Glass, R. S.; Lichtenberger, D. L. *J. Organomet. Chem.* **2009**, *694*, 2681.
(261) Gloaguen, F.; Rauchfuss, T. B. *Chem. Soc. Rev.* **2009**, *38*, 100.
(262) Yu, Z.; Wang, M.; Li, P.; Dong, W.; Wang, F.; Sun, L. *Dalton Trans.* **2008**, 2400.
(263) Felton, G. A. N.; Vannucci, A. K.; Chen, J.; Lockett, T.; Okumura, N.; Petro, B. J.; Zakai, U.; Evans, D. H.; Glass, R. S.; Lichtenberger, D. L. *J. Am. Chem. Soc.* **2007**, *129*, 12521.
(264) Vijaikanth, V.; Capon, J.-F.; Gloaguen, F.; Schollhammer, P.; Talarmin, J. *Electrochem. Commun.* **2005**, *7*, 427.
(265) Thomas, C. M.; Rüdiger, O.; Liu, T.; Carson, C. E.; Hall, M. B.; Darensbourg, M. Y. *Organometallics* **2007**, *26*, 3976.
(266) Green, K. N.; Hess, J. L; Thomas, C. M.; Darensbourg, M. Y. *Dalton Trans.* **2009**, 4344.
(267) Ibrahim, S. K.; Liu, X.; Tard, C.; Pickett, C. J. *Chem. Commun.* **2007**, 1535.
(268) Li, Z.; Ohki, Y.; Tatsumi, K. *J. Am. Chem. Soc.* **2005**, *127*, 8950.

(269) Ohki, Y.; Yasamura, K.; Kuge, K.; Tanino, S.; Ando, M.; Li, Z.; Tatsumi, K. *Proc. Natl. Acad. Sci. U.S.A.* **2008**, *105*, 7652.
(270) Barton, B. E.; Whaley, C. M.; Rauchfuss, T. B.; Gray, D. L. *J. Am. Chem. Soc.* **2009**, *131*, 6942.
(271) Rakowski DuBois, M.; DuBois, D. L. *Acc. Chem. Res.* **2009**, *42*, 1974.
(272) Wilson, A. D.; Newell, R. H.; McNevin, M. J.; Muckerman, J. T.; Rakowski DuBois, M.; DuBois, D. L. *J. Am. Chem. Soc.* **2006**, *128*, 358.
(273) Wilson, A. D.; Shoemaker, R. K.; Miedaner, A.; Muckerman, J. T.; DuBois, D. L.; Rakowski DuBois, M. *Proc. Natl. Acad. Sci. U.S.A.* **2007**, *104*, 6951.
(274) Le Goff, A.; Artero, V.; Jousselme, B.; Tran, P D.; Guillet, N.; Métayé, R.; Fihri, A.; Palacin, S.; Fontecave, M. *Science* **2009**, *326*, 1384.
(275) Appel, A. M.; DuBois, D. L.; Rakowski DuBois, M. *J. Am. Chem. Soc.* **2005**, *127*, 12717.
(276) Karunadasa, H. I.; Chang, C. J.; Long, J. R. *Nature* **2010**, *464*, 1329.
(277) EG&G Technical Services. *Fuel Cell Handbook*, 7th ed.; U.S. Department of Energy: Washington, DC, November 2004; http://www.netl.doe.gov/technologies/coalpower/fuelcells/seca/pubs/FCHandbook7.pdf (accessed November 2009).
(278) *Handbook of Fuel Cells: Fundamentals, Technology and Applications*; Vielstch, W., Lamm, A., Gasteiger, H. A., Eds.; John Wiley: Chichester, UK, 2003.
(279) White, C. M.; Steeper, R. R.; Lutz, A. E. *Int. J. Hydrogen Energy* **2006**, *31*, 1292.
(280) Grimes, C. A.; Varghese, O. K.; Ranjan, S. *Light, Water, Hydrogen: The Solar Generation of Hydrogen by Water Photoelectrolysis*; Springer: New York, 2008; Chapter 2.
(281) Crabtree, G. W.; Dresselhaus, M. S. *Mater. Res. Soc. Bull.* **2008**, *33*, 421.
(282) Schlapbach, L.; Züttel, A. *Nature* **2001**, *414*, 353.
(283) Murray, L. J.; Dincã, M.; Long, J. R. *Chem. Soc. Rev.* **2009**, *38*, 1294.
(284) Jessop, P. G.; Ikariya, T.; Noyori, R. *Chem. Rev.* **1995**, *95*, 259.
(285) Khodakov, A. Y.; Chu, W.; Fongarland, P. *Chem. Rev.* **2007**, *107*, 1692.
(286) Benson, E. E.; Kubiak, C. P.; Sathrum, A. J.; Smieja, J. M. *Chem. Soc. Rev.* **2009**, *38*, 89.
(287) Dubois, M. R.; Dubois, D. L. *Acc. Chem. Res.* **2009**, *42*, 1974.
(288) Centi, G.; Perathoner, S.; Wine, G.; Gangeri, M. *Green Chem.* **2007**, *9*, 671.
(289) Indrakanti, V. P.; Kubicki, J. D.; Schobert, H. H. *Energy Environ. Sci.* **2009**, *2*, 745.
(290) Jitaru, M.; Lowy, D. A.; Toma, M.; Toma, B. C.; Oniciu, L. *J. Appl. Electrochem.* **1997**, *27*, 875.
(291) Centi, G.; Perathoner, S.; Rak, Z. S. *Appl. Catal., B* **2003**, *41*, 143.
(292) Lukaszewski, M.; Siwek, H.; Czerwinski, A. *J. Solid State Electrochem.* **2009**, *13*, 813.
(293) Gangeri, M.; Perathoner, S.; Caudo, S.; Centi, G.; Amadou, J.; Begin, D.; Pham-Huu, C.; Ledoux, M. J.; Tessonnier, J. P.; Su, D. S.; Schlogi, R. *Catal. Today* **2009**, *143*, 57.
(294) Hori, Y.; Murata, A.; Takahashi, R. *J. Chem. Soc., Faraday Trans. I* **1989**, *85*, 2309.
(295) Hori, Y. In *Modern Aspects of Electrochemistry*; Vayenas, C. G., White, R. E., Gamboa-Aldeco, M. E., Eds; Springer: New York, 2008; Chapter 3, pp 89.
(296) Barton, E. E.; Rampulla, D. M.; Bocarsly, A. B. *J. Am. Chem. Soc.* **2008**, *130*, 6342.
(297) Surendranath, Y.; Kanan, M. W.; Nocera, D. G. *J. Am. Chem. Soc.* **2010**, *132*.
(298) Kanan, M. W.; Yano, J.; Surendranath, Y.; Dincă, M.; Yachandra, V. K.; Nocera, D. G. *J. Am. Chem. Soc.* **2009**, *132*, 13692.
(299) McAlpin, J. G.; Surendranath, Y.; Dincă, M.; Stich, T. A.; Stoian, S. A.; Casey, W.; Nocera, D. G.; Britt, R. D. *J. Am. Chem. Soc.* **2010**, *132*, 6882.
(300) Esswein, A. S.; Surendranath, Y.; Reece, S. Y.; Nocera, D. G. *Energy Environ. Sci.* **2010**, in press.

CR100246C